


Classical and quantum frequency combs for satellite-based clock synchronization

Cite as: APL Photon. 9, 100903 (2024); doi: 10.1063/5.0220546
Submitted: 26 May 2024 • Accepted: 27 September 2024 •
Published Online: 18 October 2024



Ronakraj K. Gosalia,^{1,a)}  Ryan Aguinaldo,²  Jonathan Green,² Holly Leopardi,³  Peter Brereton,³ 
and Robert Malaney^{1,b)} 

AFFILIATIONS

¹ University of New South Wales, Sydney, NSW 2052, Australia

² Northrop Grumman Corporation, San Diego, California 92128, USA

³ NASA Goddard Space Flight Center, Greenbelt, Maryland 20771, USA

^{a)} Electronic mail: r.gosalia@unsw.edu.au

^{b)} Author to whom correspondence should be addressed: r.malaney@unsw.edu.au

ABSTRACT

The next generation of space-based networks for communications, sensing, and navigation will contain optical clocks embedded within satellites. To fully realize the capabilities of such clocks, high-precision clock synchronization across the networks will be necessary. Current experiments have shown the potential for classical frequency combs to synchronize remote optical clocks over free space. However, these classical combs are restricted in precision to the standard quantum limit. Quantum frequency combs, however, which exhibit quantum properties such as squeezing and entanglement, provide pathways for going beyond the standard quantum limit. Here, we present our perspective on the prospects for practical clock synchronization in space using both classical and quantum frequency combs. We detail the current outcomes achievable with a classical frequency comb approach to synchronization, before quantifying the potential outcomes offered by quantum frequency combs. Challenges to be overcome in deploying frequency combs in space are presented, and the implications of almost-perfect synchronization for future space-based applications and experiments are discussed.

© 2024 Author(s). All article content, except where otherwise noted, is licensed under a Creative Commons Attribution (CC BY) license (<http://creativecommons.org/licenses/by/4.0/>). <https://doi.org/10.1063/5.0220546>

I. INTRODUCTION

The advent of optical clocks has enabled an unprecedented level of stability, accuracy, and precision in timekeeping,^{1,2} providing a viable solution for many applications. Indeed, optical clocks are expected to be a key enabler for next-generation metrology,³ astronomy,⁴ geodesy,⁵ navigation,⁶ and tests of fundamental physics.⁷ However, the performance of optical clocks is strictly restricted in a network by the performance of the clock synchronization scheme used. Clock synchronization across a network ensures that the reference of time is common across all devices such that network operations occur in the desired sequence. As the synchronization improves, the operations can proceed at faster rates, leading to higher network performance levels across a wide variety of network functions.⁸ Many of the applications and tests mentioned above are network based and, therefore, also enhanced by improved synchro-

nization. Although many different schemes have previously been proposed to minimize error during clock synchronization,^{9–11} it is now emerging that optical-based protocols based on frequency combs (that interconnect optical clocks) are enabling precision of clock synchronization at the standard quantum limit^{12–17} (SQL) and beyond.^{18–23}

Beyond frequency combs, other optical-based synchronization strategies currently being investigated include techniques focusing on continuous-wave (CW) laser,^{24–28} chirped frequency,²⁹ quantum correlated photons,^{30–36} and pulsed single photons,³⁷ to name a few. However, notwithstanding the merits of these other strategies, in this work we focus on the progress of classical^{12–17} and quantum^{18–23} frequency combs as, in our view, they show the most promise for practical synchronization improvement over free-space links¹⁷ especially links between satellites^{22,23} and ground-satellite configurations.^{12,14,38}

For our purposes, the distinction made between “classical” and “quantum” frequency combs will lie within whether the performance (defined by the precision in estimating the timing during clock synchronization) is limited by the SQL or the Heisenberg limit (HL). As discussed more later, the HL has a better scaling with the system resource, n , used, with, in the context of synchronization, timing accuracy improved by a factor of \sqrt{n} relative to the SQL scaling. The HL is known to be the fundamental scaling performance achievable by any system—and requires the introduction of quantum processes. The SQL is the best-case performance of a system based on classical properties of light, such as a classical frequency comb. The quantum frequency combs can instead approach the more fundamental HL. In this paper, the term quantum frequency comb will refer to a pulsed-laser system that exhibits either quadrature squeezing or quadrature entanglement (detailed further in Sec. IV). Other types of quantum frequency combs based on single photons³⁹ (which are also called “quantum optical microcombs”) are beyond the scope of this work.

It is our view that over size, weight, and power (SWaP) constrained links, the quantum frequency comb can provide an efficient solution for next generation satellite networks that require fundamental scaling performance. We envisage a scenario where both classical and quantum frequency combs co-exist throughout the network, the latter only being used when absolutely required on certain links. The architecture shown in Fig. 1 summarizes this future perspective. The delivery, and performance of the classical and quantum frequency combs that form the synchronization links of this space-based architecture, forms the focus of our paper.

The rest of this paper is organized as follows: in Sec. II, we provide contextual details on the recent progress in timekeeping and clock synchronization and compare the fundamental precision advantage of quantum-enhanced clock synchronization. We provide details of classical frequency combs in Sec. III, including the operating principles, a comparison of recent satellite-based experiments, and highlight the key challenges ahead. In Sec. IV, we highlight the theory, recent progress, and challenges of quantum frequency combs, and Sec. V includes our outlook on the field. Finally, Sec. VI presents our conclusions.

II. BACKGROUND

In this section, we briefly discuss the recent progress in optical clocks and synchronization. Furthermore, trade-offs between classical and quantum clock synchronization schemes are discussed. As mentioned earlier, satellite-based optical clocks would enable a new frontier for next-generation communications, navigation, and sensing applications. All these applications will require a network of clocks. This network would also need time-transfer capabilities at precision levels that match, and ideally exceed, the timekeeping precision of the clocks. Hence, as the field of optical clocks progresses, so to must the field of clock synchronization.

A. Fractional frequency instability and timing deviation

In the literature, the term fractional frequency instability (FFI) is also referred to as the “fractional frequency uncertainty,” the

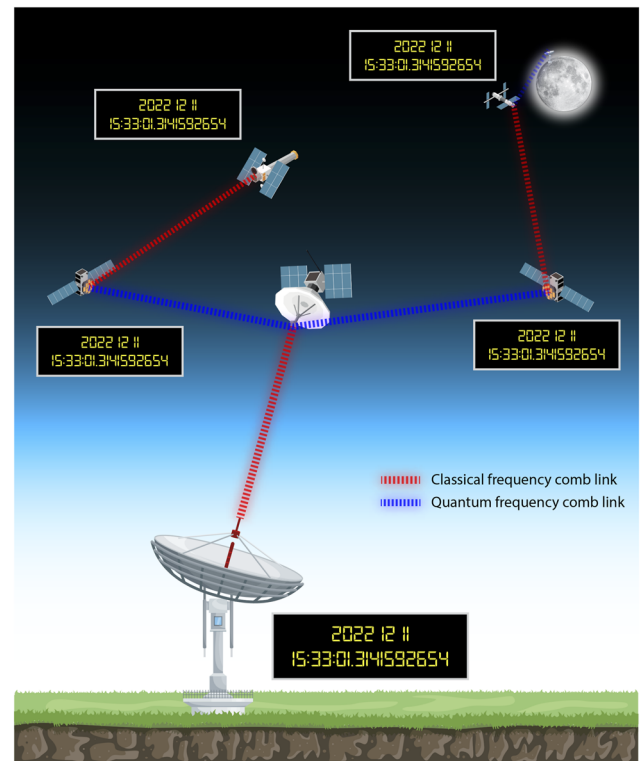


FIG. 1. Our perspective on the next-generation network of highly synchronized satellite-based clocks, which will be the backbone infrastructure for many applications including communications, navigation, and sensing. A mixture of classical and quantum frequency comb-based links are expected based on current research. The quantum approach provides, in principle, resource efficiencies for high-precision clock synchronization, which are important in low SWaP (e.g., satellite) scenarios (as discussed in Sec. II). However, at present, the quantum approach is limited to short-range inter-satellite links where the detrimental impact of loss and noise can be contained (as detailed in Sec. IV). On the contrary, over long-range links such as ground-satellite, the classical approach may be preferred due to implementation simplicity, but this would be at the cost of a higher SWaP demand (see Sec. III). An all-quantum approach would maximize the resource efficiencies across the entire network, but many implementation challenges currently exist, which are open directions of research.

“Allan deviation,” the “systematic uncertainty,” or simply as the “uncertainty.” Technically, the FFI is the average two-sample difference of the average fractional frequency and is a useful metric for comparing between different clocks and clock synchronization techniques.⁴⁰ The fractional frequency is a ratio of the difference between the oscillating frequency and the nominal frequency divided by the nominal frequency. In the context of clocks, the FFI is a measure of the frequency stability of a clock, and a smaller value of FFI represents a higher clock stability and time-keeping precision. Across the literature, however, different methods are used to calculate the FFI and sometimes the method used is not specified, which makes comparisons challenging. Here, we begin by detailing the three most popular definitions for the FFI as outlined in IEEE 1139-2022,⁴⁰ Riley and Howe,⁴¹ and Rubiola and Vernotte.⁴²

An instantaneous signal produced by the oscillations in a clock can be described as a time-dependent amplitude, $S(t)$, given by

$$S(t) = S_0 \cos(2\pi\nu_0 t + \phi(t)), \quad (1)$$

where S_0 is the peak amplitude, ν_0 is the nominal oscillating frequency of the clock, and $\phi(t)$ is the instantaneous phase of the clock. When characterizing clocks and clock synchronization techniques, we are concerned with the stability of two parameters: the frequency and the phase. Instabilities in the frequency are calculated via the instantaneous fractional frequency, $y(t)$, which is given by

$$y(t) = \frac{\nu(t) - \nu_0}{\nu_0} \equiv \frac{1}{2\pi\nu_0} \frac{d\phi(t)}{dt}, \quad (2)$$

where $\nu(t)$ is the instantaneous frequency of the clock. Instabilities in the phase are calculated via the instantaneous timing deviation, $x(t)$, that is given by

$$x(t) = \frac{\phi(t) - \phi_0}{2\pi\nu_0}, \quad (3)$$

where ϕ_0 is the nominal phase (often assumed $\phi_0 = 0$). It should be noted that $\phi(t) - \phi_0$ represents the instantaneous phase offset, which is the measured parameter in some experiments (for more details on phase synchronization, see Ref. 43 and references therein). We also note that $y(t)$ and $x(t)$ are related to each other via

$$y(t) = \frac{dx(t)}{dt}. \quad (4)$$

An experimenter has the choice regarding whether to measure $y(t)$, $x(t)$, or both. In practice, samples of $y(t)$ or $x(t)$ are collected at discrete time intervals separated by a fixed sample period τ_0 , giving a collection of samples $[\bar{y}_1, \bar{y}_2, \dots]$ and $[\bar{x}_1, \bar{x}_2, \dots]$, respectively. Each sample can be described as an average quantity over τ_0 , namely,

$$\bar{y}_k = \frac{1}{\tau_0} \int_{t_k}^{t_{k+1}} y(t) dt \quad \text{and} \quad \bar{x}_k = \frac{1}{\tau_0} \int_{t_k}^{t_{k+1}} x(t) dt, \quad (5)$$

with $t_k = (k - 1)\tau_0$ and $k \in [1, 2, \dots]$ is the sample index. It should also be noted that the discrete version of Eq. (4) used in practice, namely,

$$\bar{y}_k = \frac{\bar{x}_{k+1} - \bar{x}_k}{\tau_0}. \quad (6)$$

After $M \gg 1$ samples are collected, the FFI is calculated. The first method for computing the FFI, which we henceforth denote as $\text{FFI}^{(0)}$, calculates the average difference between adjacent samples, and is given by

$$\begin{aligned} \text{FFI}^{(0)} &= \left[\frac{1}{2(M-1)} \sum_{k=1}^{M-1} (\bar{y}_{k+1} - \bar{y}_k)^2 \right]^{\frac{1}{2}} \\ &= \left[\frac{1}{2(M-1)\tau_0^2} \sum_{k=1}^{M-1} (\bar{x}_{k+2} - 2\bar{x}_{k+1} + \bar{x}_k)^2 \right]^{\frac{1}{2}}. \end{aligned} \quad (7)$$

The method in Eq. (7) is also referred to in the literature as the ‘‘Allan deviation.’’ However, Eq. (7) has been largely superseded by

the ‘‘overlapping Allan deviation,’’ referred to henceforth as ADEV, which uses the difference between non-adjacent samples to improve the confidence in the FFI estimate. The time-distance between the non-adjacent samples is an integer multiple of τ_0 , which we denote as $m\tau_0$, where $m \in \mathbb{Z}^+$. ADEV is given by

$$\begin{aligned} \text{ADEV} &= \left[\frac{1}{2m^2(M-2m+1)} \sum_{j=1}^{M-2m+1} \left\{ \sum_{k=j}^{j+m-1} (\bar{y}_{k+m} - \bar{y}_k) \right\}^2 \right]^{\frac{1}{2}} \\ &= \left[\frac{1}{2m^2(M-2m+1)\tau_0^2} \sum_{k=1}^{M-2m+1} (\bar{x}_{k+2m} - 2\bar{x}_{k+m} + \bar{x}_k)^2 \right]^{\frac{1}{2}}. \end{aligned} \quad (8)$$

Finally, a third method exists called the ‘‘modified Allan deviation,’’ referred to henceforth as MDEV. The MDEV has the advantage of acting as an algorithmic filter to help in distinguishing between white noise and flicker phase noise, as discussed later in this section. MDEV extends ADEV using the same time-distance between non-adjacent samples of $m\tau_0$ and is given by

$$\begin{aligned} \text{MDEV} &= \left[\frac{1}{2m^4(M-3m+2)} \right. \\ &\quad \left. \times \sum_{j=1}^{M-3m+2} \left\{ \sum_{i=j}^{j+m-1} \left(\sum_{k=i}^{i+m-1} (\bar{y}_{k+m} - \bar{y}_k) \right) \right\}^2 \right]^{\frac{1}{2}} \\ &= \left[\frac{1}{2m^4(M-3m+2)\tau_0^2} \right. \\ &\quad \left. \times \sum_{j=1}^{M-3m+2} \left(\sum_{k=j}^{m+j-1} (\bar{x}_{k+2m} - 2\bar{x}_{k+m} + \bar{x}_k) \right)^2 \right]^{\frac{1}{2}}. \end{aligned} \quad (9)$$

When $m = 1$, Eqs. (7)–(9) are all equal. In addition, depending on the size of m , $\text{FFI}^{(0)}$ can be very different to ADEV and MDEV over the same collected samples. It should be noted, when computing ADEV and MDEV, m is incrementally increased from $m = 1$ to $m = M$ until the computation of FFI begins to diverge due to systematic noise.

To aid, as shown in Fig. 2, we have provided a visual of an example experiment where $M = 8$ samples of \bar{y} are collected. Here, the difference between $\text{FFI}^{(0)}$ and ADEV are shown when $m = 2$. The integration time, denoted by τ , is the duration of the sampling window in seconds. When $\text{FFI}^{(0)}$ is computed, $\tau = \tau_0$, and when ADEV or MDEV are computed, $\tau = m\tau_0$. It is important that the FFI is always reported alongside τ due its dependence on m and τ_0 .

Unfortunately, across the literature, there is an inconsistency in that some studies report the $\text{FFI}^{(0)}$, while others report the ADEV or MDEV. To make matters worse, some studies do not make clear whether they are reporting the $\text{FFI}^{(0)}$, ADEV, or MDEV. In this paper, we will stipulate whether $\text{FFI}^{(0)}$, ADEV, or MDEV were used in a referenced work when it is clear. However, when a referenced work has failed to stipulate the specific form used, we will term the reported value as simply the ‘‘FFI.’’ As it will be clear from the context in which it is used, we will also occasionally use the term ‘‘FFI’’ as a means to refer to $\text{FFI}^{(0)}$, ADEV, or MDEV.

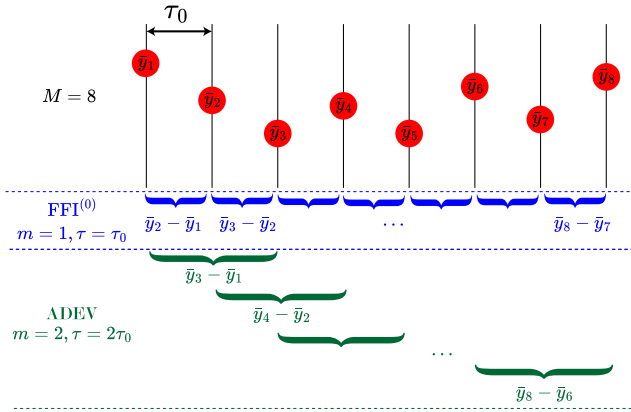


FIG. 2. Example experiment with $M = 8$ samples of \bar{y} that are separated in time by the fixed sampling period τ_0 . Two different methods for computing the FFI are pictorially shown. The first, $\text{FFI}^{(0)}$, calculates the average difference between adjacent samples of \bar{y} . The second, ADEV uses non-adjacent samples—here, as an example, we have fixed $m = 2$ such that the time duration between the non-adjacent samples is $2\tau_0$. The integration time, τ , is the duration of each sampling window; in the above-mentioned example, with $\text{FFI}^{(0)}$, $\tau = \tau_0$, and with ADEV, $\tau = 2\tau_0$.

The different definitions of FFI exist to help distinguish between various sources of noise in real experiments,⁴⁴ which, in the context of clocks and clock synchronization, are white noise, flicker noise, and random-walk.^{40,41} These noise sources can be present in \bar{x} and \bar{y} measurements, giving rise to phase-modulation (PM) and frequency-modulation (FM), respectively. White noise is uncorrelated random noise, which has a flat spectral density profile. Flicker noise has a spectral density given by f^{-1} , where f is the frequency, and random-walk has a spectral density given by f^{-2} . When either of these noise sources dominate the measurement, the influence can be observed via the gradient of the log-log plot of FFI vs τ . The various gradient values for each noise source are presented in Table I. For example, when white PM noise is dominant, the $\text{FFI}^{(0)} \propto \tau^{-1}$, $\text{ADEV} \propto \tau^{-1}$, and $\text{MDEV} \propto \tau^{-3/2}$. In a state-of-the-art clock synchronization experiment, white PM was the dominant noise source from $0 \leq \tau \leq 0.5$ s, and when $\tau > 0.5$ s, flicker PM noise was dominant.¹⁷ It should be noted that the distinction between white PM and flicker PM can only be made with MDEV, and this is the reason for the general preference for MDEV over the other definitions of FFI. Furthermore, the noise sources also limit the maximum τ in a clock synchronization experiment—the maximum τ is when the dominant noise source is flicker FM noise and the computation of

TABLE I. Coefficient α of $\text{FFI} \propto \tau^\alpha$ for the most common sources of noise. It should be noted that α is different for white PM and flicker PM when MDEV is used compared to $\text{FFI}^{(0)}$ and ADEV, and for this reason, MDEV is preferred to distinguish between these two sources of noise.⁴¹

FFI method	White PM	Flicker PM	White FM	Flicker FM	Random-walk FM
$\text{FFI}^{(0)}$ and ADEV	-1	-1	-1/2	0	1/2
MDEV	-3/2	-1	-1/2	0	1/2

FFI no longer converges to zero. FFI measurements beyond the maximum τ are not trusted. The total measurement duration, T , sets $\tau = T/2$ for ADEV, and $\tau = T/3$ for MDEV.

Although the FFI provides a useful metric for comparing the stability of clocks, in clock synchronization we are interested in the timing error between clocks. To this end, we introduce the timing deviation (TDEV), which quantifies the time stability of a clock. The TDEV is related to the FFI via

$$\text{TDEV} = \frac{\tau}{\sqrt{3}} \text{MDEV}, \tag{10}$$

with units of seconds. The timing error between clocks, denoted throughout this work by the standard deviation $\sigma_{\Delta t}$, is given by

$$\sigma_{\Delta t} = \sigma_{\text{excess}} + \text{TDEV}, \tag{11}$$

where σ_{excess} is the sum of any initial synchronization issues between the clocks as well as any environmentally induced and frequency drift-related timing offsets. In the recent state-of-the-art clock synchronization experiment, $\sigma_{\text{excess}} \approx 0$ was achieved using classical frequency combs and sophisticated signal processing techniques (discussed further in Sec. III E) when $0 \leq \tau \leq 1$ s.¹⁷ Within this region, $\sigma_{\Delta t} \equiv \text{TDEV}$ and white PM noise dominated the system yielding $\text{TDEV} \propto \tau^{-1/2}$ —also referred to in the literature as the “quantum-limited white noise floor.”^{17,45} TDEV and FFI measurements are at the SQL when white PM is the only noise source in the system.

In our perspective, future satellite-based clock synchronization techniques should aim to achieve an MDEV of $< 10^{-18}$ within $\tau \leq 100$ s for satellite-based clock synchronization. At this stability, a TDEV in the sub-femtosecond regime would be achievable using classical and quantum frequency combs (with femtosecond pulse duration) operating at the white noise floor. An integration time of less than 100 s would also ensure compatibility with the typical viewing time-window of a low-Earth-orbit (LEO) satellite.⁴⁶

B. Optical clocks on ground and in space

Current optical clock technologies can achieve an FFI of order 10^{-18} in ground-based laboratory settings, surpassing the performance of cesium-based atomic clocks. This level of stability has been achieved in experiments that are focused largely on lowering the FFI by overcoming technical issues such as second-order Doppler shifts,⁴⁷ thermal radiation,⁴⁸ and more.^{48,49} Some examples of architectures include the strontium ion optical lattice (FFI of 10^{-18} at $\tau = 10^4$ s⁵⁰ and ADEV of 4×10^{-19} at $\tau = 5 \times 10^3$ s⁵¹) and the ytterbium ion optical lattice (FFI of 4×10^{-19} at $\tau = 10^5$ s⁵²). As the field of optical clocks matures, the focus will shift to achieving a shorter duration of τ for a given level of FFI, in addition to lowering the FFI. Furthermore, future optical clocks will be placed in orbit around the Earth to escape the noise effects due to Earth’s gravitational fluctuations, which is a limiting factor for MDEV of 10^{-18} at $\tau \leq 100$ s at present.^{7,53} Satellite-based optical clocks will also aid spacecraft navigation by avoiding communication delays with Earth on corrections to trajectories. Optical clocks in space will also be used for the global dissemination of time and the re-definition of the second.

However, current optical clocks have high SWaP demands—satellite-based solutions will require miniaturization and

radiation hardening, and considerable research is already under way toward these directions.⁵³ Satellite-based optical and atomic clocks is a research direction that is receiving considerable attention by various space agencies, which includes the National Aeronautics and Space Administration and their Deep Space Atomic Clock project,^{54–56} the European Space Agency and their Atomic Clocks Ensemble in Space,^{57,58} the German aerospace center's project COMPASSO,⁵⁹ and the Chinese Space Laboratory's Tiangong-2 cold atomic clock.⁶⁰ With the exception of COMPASSO, these projects are using atomic clocks although the findings should also translate to optical clock technologies. In the near-future, when a network of satellite-based optical clocks are deployed, we will require a clock synchronization scheme that is able to share time and frequency information with stability at an FFI better than the optical clocks themselves and also within a reasonably short τ duration that is suitable for satellite links.

For clarity, in this manuscript, we denote clock architectures based on optical transitions as “optical clocks,” whereas architectures based on microwave transitions are called “atomic clock.” Although we highlight that throughout the literature optical clocks are sometimes also referred to as “optical atomic clocks,” and atomic clocks are sometimes referred to as “microwave atomic clocks.”

C. Clock synchronization schemes without frequency combs

Current commercially available clock synchronization protocols, such as global positioning system (GPS) common-view time transfer^{61,62} and GPS carrier phase,⁶³ use a microwave carrier as the signal. However, although these techniques are suitable for synchronizing atomic clocks, they are unable to reach an FFI of 10^{-18} (and lower), which is required for a network of optical clocks.⁵³ For instance, the GPS carrier-phase protocol can achieve an MDEV of 10^{-16} at $\tau = 10^5$ s.⁶⁴ Similarly, the carrier-phase two-way satellite time and frequency transfer schemes also suffers from the same threshold.^{63,65,66} While efforts are made to improve the FFI below this level,⁶⁷ the microwave-based carrier is a significant limiting factor. An opportunity exists for lowering the FFI by increasing the carrier frequency from microwave to optical—this can be understood as an increase to ν_0 in Eqs. (2) and (3), which would lower $\gamma(t)$ and $x(t)$ and, in turn, the FFI. In practice, however, optical signals are more sensitive to loss and noise in free space than microwave signals, which complicates the matter. Fortunately, recent experiments with optical signals are showing progress toward the required FFI levels. These experiments also reveal practical strategies for overcoming loss and noise issues that may be translated to satellite-based implementations in the near-future.

A potential optical-based method is the coherent optical frequency transfer (OFT). OFT uses an optical continuous-wave (CW) laser, which is phase-locked to a clock, as the signal. The laser is transmitted to a remote site and interrogated with another CW laser that is locked to a different clock. By extracting the phase difference between the two CW laser signals, the TDEV between the clocks can be determined. However, the OFT protocol is highly sensitive to phase noise issues induced by atmospheric turbulence. OFT is also sensitive to amplitude noise, which reduces the signal-to-noise ratio and causes signal drop-outs. Amplitude noise is a result of beam wandering, scintillation, and deep fading in a free-space

channel.²⁷ Without dedicated noise-compensation strategies, phase and amplitude noise significantly limit the maximum τ achievable in OFT over free space and, in turn, limit the minimum FFI achievable.

Recently, an OFT experiment conducted by Gozzard *et al.*⁶⁸ used a 1532 nm narrowband (<100 Hz bandwidth) laser transmitted over a 2.4 km free-space terrestrial link. In this experiment, an MDEV of 6.1×10^{-21} at $\tau = 300$ s⁶⁸ was achieved. This level of FFI exceeds the requirement for synchronizing optical clocks and satisfies our criteria for satellite-based clock synchronization (as shown in Fig. 3). However, it is important to note that the performance strongly relies on the use of ultra-precise phase stabilization and amplitude noise suppression systems. Particularly, an imbalanced Michelson interferometer, an acousto-optic modulator, a bidirectional erbium-doped fiber amplifier, and an adaptive optics unit were among some of the additional hardware components that were required to reduce the MDEV of 10^{-15} at $\tau = 10^4$ s.

In contrast to OFT, a pulsed laser techniques can have a large “ambiguity range,”^{28,69} which allow it to be more robust against atmospheric turbulence and signal drop-outs during deep fades.⁷⁰ Time transfer by laser link (T2L2) is one such optical protocol that is based on the principles of a laser-ranging technique that collect time-of-flight measurements.⁷¹ In T2L2, several laser pulses are transmitted between a satellite and one or more ground stations and detected using photodetection devices and time-tagging units. These laser pulses are of short duration and asynchronously transmitted from the ground stations to the satellite, with a fraction of them returned back to the ground stations. The ground stations record the start and return time of each pulse, while the satellite records the arrival time in the temporal reference frame of the on-board clock. A microwave carrier is then used to share the start, return, and arrival times and calculate the TDEV. Unfortunately, the current implementations of the T2L2 protocol have not been able to achieve an MDEV $\leq 10^{-18}$ at $\tau \leq 100$ s.

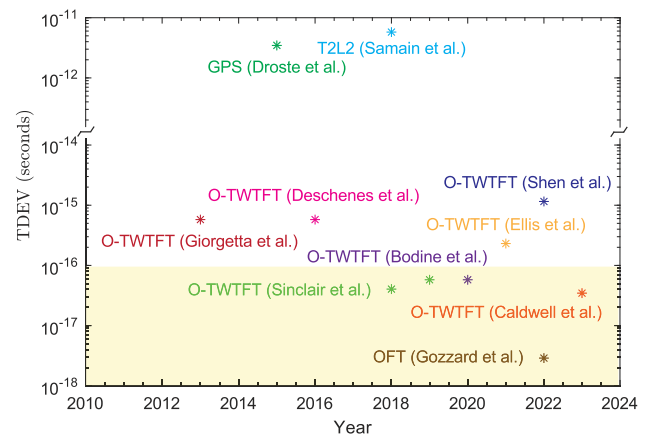


FIG. 3. Historical comparison of different state-of-the-art free-space clock synchronization studies. It should be noted that the TDEVs plotted are the values reported at $\tau = 100$ s from the respective studies. In yellow, we highlight the studies that have achieved an MDEV of $\leq 10^{-18}$ at $\tau \leq 100$ s (i.e., a TDEV of $\leq 10^{-16}$ s), which is our criteria for the performance required to synchronize satellite-based optical clocks. It is evident that some recent studies satisfy our criteria.

In a recent field experiment, T2L2 was tested between the Jason 2 satellite and a single ground station.^{25,26} In this particular test, the FFI achieved was of order 10^{-13} at $\tau = 100$ s.⁷² Although, the FFI can be reduced to an FFI of 10^{-17} at $\tau = 1$ day,⁵³ this would be unsuitable for links with LEO satellites. The main issue with T2L2 is that photodetection devices have a relatively slow response rate, which limits the maximum sampling rate and in turn precision of the final TDEV measurements.²⁸ Although, in principle, T2L2 should reach an FFI of 10^{-17} at $\tau = 300$ s²⁴ and an MDEV of 10^{-17} at $\tau = 1$ s.⁷³

A final point of interest is that both the T2L2 and the OFT present two different optical-based methods for clock synchronization. From a fundamental physics perspective, T2L2 follows the time-of-flight method and relies on the precise comparison of the departure and arrival times of different sets of pulses to estimate the TDEV between two different clocks, whereas OFT operates under the phase method and focuses instead on the relative phase difference between a local and remote narrowband optical signal. Both methods, in theory, should be able to yield the same level of FFI for a given τ (discussed further in Sec. IV B) but, in practice, they require different hardware setups for operation over free-space links. As discussed in Secs. III and IV, classical and quantum frequency combs provide an alternative pathway to time-of-flight and phase-based clock synchronization, and recent experiments are indicating that these approaches may also demand less hardware in practice. Less complex hardware should translate to lower SWaP demands, which are highly desirable in space.

A visual summary of the performance of various state-of-the-art clock synchronization techniques including a classical frequency comb-based technique known as optical two-way time and frequency transfer (O-TWTFT), discussed in Sec. III E, is shown in Fig. 3, with our satellite-based clock synchronization criteria highlighted in yellow.

D. One-way vs two-way time transfer

Another point of distinction between different clock synchronization techniques over free space are the one-way and two-way transfer approaches.^{61,74} In the one-way approach, there exists one transmitter and one or more receivers. The transmitter could be a ground station or a satellite that generates a signal with timing and or frequency information about the transmitter clock. The receiver/s would capture the signal, decode, and compare against the same information from a local clock. This approach is technologically simple and could cater for a large network, but there exist some implementation challenges. A challenge for the one-way method is that the location of the transmitter and receiver/s need to be known as precisely as possible before the exchange of signals takes place. The path distance between the transmitter and the receiver/s are needed to remove the path-based signal delay in the final calculation of TDEV. When the transmitter or receiver/s are not stationary, e.g., satellites, changes in path delay will contribute phase noise to the final TDEV estimate. Another key limiting factor for the one-way approach is that random path-length variations caused, for instance, by atmospheric turbulence would also contribute phase and amplitude noise, as discussed in Sec. II C. Finally, variations in the refractive index across the channel will affect the propagating speed of the signals and also impact path-delay. For

instance, the troposphere near the Earth's surface increases the effective path delay by 1 ns per km,⁷⁴ which would need to be accounted for in ground-satellite links. For the successful operation of a one-way transfer scheme, the path-based delays must be determined. This can be aided by determining the position of all sites *a priori*, ensuring all sites remain relatively stationary and characterizing the refractivity of the channel during the transmission of signals.⁷⁴

In contrast, a two-way transfer scheme does not depend as strongly on path-based delays.⁷⁵ Here, usually an intermediary satellite is used between two ground stations. The ground stations transmit signals to the satellite, and the satellite forwards the signal from each ground station to the other. In theory, the position of any given satellite or ground station/s are no longer needed because all signals will travel from a ground station to the satellite and back, making path-based delays common across all signals. However, path-based noise will cancel only when the channel between the satellite and ground stations is reciprocal, i.e., the effect of the channel in one direction can be canceled by propagation in the opposite direction. However, ground-to-satellite and satellite-to-ground channels are asymmetric since the former experiences the majority of atmospheric turbulence near the transmitter, while the latter experiences turbulence at the receiver. Recent simulation^{45,73,76} and experimental⁷⁷ studies have indicated that turbulence will limit the minimum TDEV achieved by all techniques. Although, a classical frequency comb-based technique known as optical two-way time and frequency transfer (O-TWTFT) is showing promising steps toward overcoming the effects of turbulence by using Kalman filtering.^{17,45}

Both the one-way and two-way methods can be setup in various configurations, which include exclusively between satellites without ground station/s. In this case, channel reciprocity may be satisfied due to there being negligible atmospheric turbulence in, for instance, LEO. Furthermore, the simpler one-way method may also suffice in LEO links.

E. Classical vs quantum

T2L2, OFT, and O-TWTFT all use properties of light that pertain to classical physics. The best-case FFI (and TDEV) achievable by any of these "classical" techniques will be the SQL.⁷⁸ The SQL is technically a scaling in the standard deviation of a measurement given by $\sigma \propto 1/\sqrt{n}$, where σ is the standard deviation and n is the number of resources used. In the context of clock synchronization, the FFI (and TDEV) when classical techniques are employed scale as $1/\sqrt{n}$, with n being the number of signal photons captured during τ .

Quantum physics provides a new scaling of the standard deviation by using "non-classical" correlations within the properties of light.⁷⁹⁻⁸⁶ Quantum states can be used to approach the HL, which is a scaling in the standard deviation given by $\sigma \propto 1/n$, a \sqrt{n} improvement relative to the SQL. There are two ways to interpret the HL: (1) for a given level of σ , a quantum state may use less n than a classical or (2) for a given amount of n , a quantum state may achieve lower σ than a classical. We define the inverse of the standard deviation as the precision.

To see the distinction between the SQL and the HL, we have presented a visualization of the precision vs resources in Fig. 4.

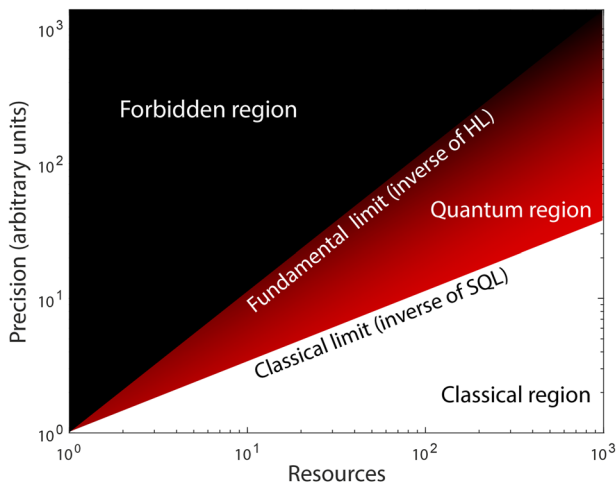


FIG. 4. Precision vs the number of resources (e.g., photons) trade-off for measurement strategies that use classical and quantum signals. All clock synchronization techniques that use the classical properties of light would operate in the classical region with a best-case performance at the SQL. On the other hand, quantum frequency combs can exploit non-classical properties, such as quadrature-squeezing and quadrature-entanglement, to operate within the quantum region. We define performance anywhere in the quantum region as “quantum advantage.”

In resource-constrained settings, such as on-board satellites, the precision-to-resource trade-off is an important consideration. In this work, we define a performance anywhere within the quantum region shown in Fig. 4 as “quantum advantage” because higher precision is achieved for a given number of resources relative to classical.

III. CLASSICAL FREQUENCY COMBS

In this section, we provide focus on clock synchronization using classical frequency combs and discuss the generation and operating principles of a mode-locked laser (MLL)—a popular choice for generating classical frequency combs. We also discuss some challenges toward noiseless operation and some findings from recent satellite-based experiments with MLLs. This section serves as an overview of the field in general and outlines progress toward SWaP optimizations.

A. Generating and characterizing classical frequency combs

In the literature, the term (classical) “frequency combs” is often synonymous in usage with “MLL.”⁸⁷ This is because MLLs were the original source of classical frequency combs in the early 2000s when they were used to perform read-outs of an optical clock by coherently and precisely converting the clock’s optical cycles into measurable microwave signals.^{88–90} Since then, applications for MLLs have widened and techniques for generating and stabilizing MLLs has also matured considerably.^{91–94} MLL-based combs remain a popular choice for comb generation, with the focus recently shifting toward balancing the trade-off between producing a wide spectral bandwidth, high frequency resolution, and a low SWaP footprint, on the

road to widespread commercialization.⁹⁵ Although there are other methods for generating classical frequency combs that are based on nonlinear processes, such as Kerr combs, electro-optic combs, and quadratic combs,^{95–99} we focus mainly on MLL-based classical frequency combs.

An MLL-based frequency comb starts as a single-frequency continuous-wave laser that is passed through a resonant cavity and stabilized via active or passive mode-locking. The optical-frequency modes of this comb are mode-locked during the stabilization process, which ensures that they are equidistant in the frequency domain, phase-coherent in the time domain, and share a common phase evolution that is deterministic.⁹³ Mode-locking is a resonant phenomenon that has been developed over many decades.^{88,100,101} In principle, a single-frequency laser is converted into a train of ultra-short duration pulses by repeatedly passing the laser through a resonator in a cavity. Each cavity round trip produces pulses that shorten in the time domain, with successive passes, and simultaneously widen in the frequency domain. The round trips continue until the cavity characteristics prevent further time-shortening and spectrum-expansion and, at this point, the pulses escape the cavity.⁸⁸ MLLs are typically ultra-short in duration ($T_0 \approx 10^{-14}$ s, where T_0 is the pulse duration as shown in Fig. 5), have a wide spectral bandwidth (order 1000 nm for octave-spanning combs), and relatively high peak output power (order 10 mW). These three characteristics are highly desirable for high-precision sensing applications including clock synchronization.^{20,102}

In principle, MLLs are simple to operate as there are only two parameters in the frequency domain that can be tuned. These parameters are as follows: the laser repetition rate (f_r) and the carrier-envelope offset frequency (f_0). These two parameters can

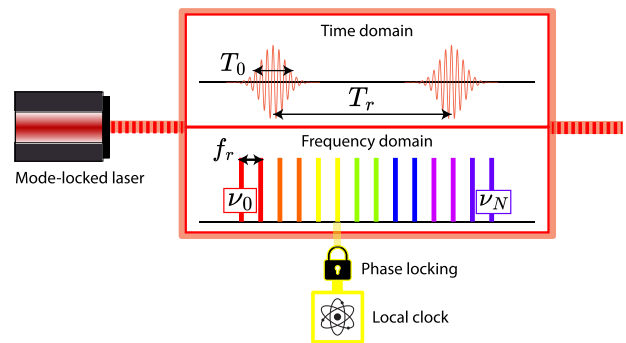


FIG. 5. Frequency and time domain representations of a classical frequency comb based on an MLL. In the optical frequency domain, the comb is a collection of optical modes denoted as ν_N with mode spacing f_r (the repetition rate of the laser). In the time domain, the comb is a periodic train of optical pulses with pulse period $T_r = 1/f_r$. For clock synchronization, one of the frequency comb modes will be first phase-locked to the transition of an optical clock. Due to the coherence shared between all frequency comb modes, all modes will in turn become phase-locked to the optical clock as well. Then, the frequency comb will be transmitted over free-space to a remote site. At the remote site, interferometry is used to compare the transmitted comb to a “receiver” comb (that is phase-locked to a receiver optical clock). Interferometry will reveal differences in the phase and/or time-of-flight information between the two combs, which is in turn linked to the TDEV between the transmitter’s and receiver’s clocks.¹²

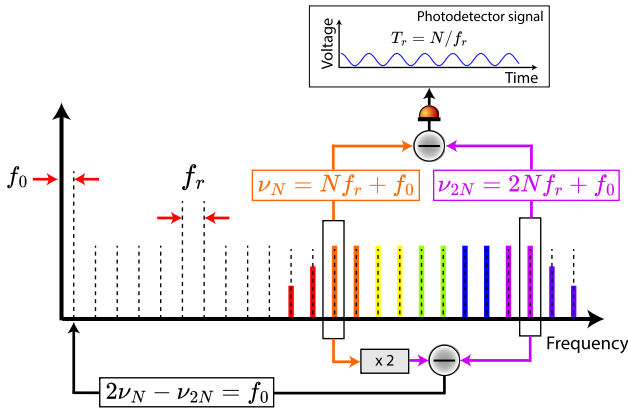


FIG. 6. Visualization of the MLL-based frequency comb stabilization process. At the bottom, the self-referencing technique for determining the offset frequency, f_0 , is shown. At the top, we show the amplitude modulation technique, which consists of an optical photodetector that is used to extract an electronic signal whose period, T_r , is related to the frequency comb mode spacing f_r . Real MLL outputs exhibit an approximately Gaussian shape in the frequency domain centered at an optical frequency with a bandwidth that spans at least one octave (for self-referencing).¹²

be considered as the two degrees of freedom of a frequency mode, denoted by ν_N , since

$$\nu_N = Nf_r + f_0, \tag{12}$$

which is referred to as the “frequency comb equation,” and $N \in \mathbb{Z}^+$ is the mode index.^{87,93} We can equivalently describe an MLL in the time-domain, but in this case, we have the following three parameters: the pulse duration (T_0), the pulse-to-pulse period ($T_r = 1/f_r$), and the pulse-to-pulse phase slip between the carrier and envelope ($\Delta\phi_{ceo} = 2\pi f_0/f_r$). In Figs. 5 and 6, we have shown visuals describing these parameters to aid. Ultimately, the sustained operation of an MLL requires tight monitoring and control of the aforementioned parameters during the generation stage—the tighter the control, the more stable the generated pulses are, and the lower the FFI (and TDEV) will be over free space.

B. Stabilizing MLLs and suppressing noise

The parameters of an MLL are typically measured and controlled using feedback loops.⁹³ First, to measure f_r , an optical photodetector is used to detect the amplitude modulation of a group of pulses (referred to as a pulse train), which in turn produces an electronic train of microwave Fourier harmonics at $f_n = nf_r$, where $n \in \mathbb{Z}^+$. One example where only two modes were interrogated is shown in Fig. 6, although in practice the entire spectrum of modes could be analyzed.¹² Second, f_0 is measured at optical frequencies by using the self-referencing method (also called $f - 2f$ interferometry¹⁰³). In sensing applications, it is essential that f_r , f_0 , T_r , $\Delta\phi_{ceo}$, and τ are stable during operation. Particularly in the clock synchronization context, it is highly desirable that $10 \text{ MHz} \leq f_r \leq 1 \text{ GHz}$, as this range allows for a commercial-of-the-shelf photodetection units for use in measurement schemes, such as linear optical sampling.^{93,104}

Unfortunately, due to various sources of noise that can arise during the generation stage, real-time measurements of the parameters (i.e., f_r and f_0 mainly) are required for optimum performance. A negative feedback loop based on tuning the cavity length is one common approach for noise suppression.^{105,106} For instance, in a fully stabilized MLL (where the parameters are fixed), T_r is precisely the round-trip time for a single pulse through the laser cavity. However, changes in the cavity length even down to an optical wavelength in length (i.e., nanometer-scale) will impact T_r of the output MLL, causing a phenomenon termed timing jitter.^{105,107} Cavity length changes will impact the temporal spacing between successive pulses as they leave the cavity. Timing jitter is unfortunately a common issue and can arise due to many factors; here, we list some common sources and strategies. Sources of timing jitter include intra-cavity amplified spontaneous emission,^{108,109} cavity dispersion,¹¹⁰ intensity fluctuations,¹¹¹ and slow saturable absorber recovery time¹¹² (in passive mode-locked combs). Several techniques for controlling timing jitter also exists and these include the phase detector method,¹¹³ balanced optical cross correlation,^{114,115} optical heterodyne,¹¹⁶ delayed optical heterodyne,¹⁰⁷ intrinsic noise optimization,¹¹¹ and phase locking.¹¹⁷ Recently, the balanced optical cross-correlation method is gaining popularity due to its superior performance.¹¹⁴

Over the past few decades, models for timing jitter-related noise have improved considerably.^{118–122} These models have helped focus future noise suppression strategies by revealing the main contributing factors of timing jitter. Namely, it was found that shortening T_0 (the pulse duration) and eliminating cavity dispersion are the best strategies. Shortening T_0 helps reduce the impact of amplified spontaneous emissions, while eliminating cavity dispersion helps to minimize the intensity- and frequency-related fluctuations in the output MLL.¹¹⁴ Using these insights, Song *et al.*¹¹⁴ were able to produce an MLL with an ultra-low timing jitter of 175 as on an ytterbium fiber-based frequency comb. Their noise-suppression technique was based on balanced optical cross correlation;¹¹⁴ however, due to limitations in their setup, the output MLL had a maximum $f_r \leq 80 \text{ MHz}$ since the timing jitter was considerably worse at higher f_r . More recently, Ma *et al.*,¹²³ was able to extend this performance on the same ytterbium-fiber comb to $f_r \leq 750 \text{ MHz}$ using an electro-optic modulator and a piezoelectric transducer units and have also inspired other studies.¹²⁴

Since T_0 of a typical MLL is at the order of the duration of a few optical cycles, instabilities in $\Delta\phi_{ceo}$ and in turn the f_0 (referred to as phase noise) are common.¹⁰⁶ Particularly, fluctuations in $\Delta\phi_{ceo}$ during operation would induce relative phase-shifts between pulses, reducing the coherence between pulses. These fluctuations are a result of changes between the group and phase velocity of a pulse as it transits the cavity and can arise due to intra-cavity amplified spontaneous emission, cavity loss, pump noise, and fluctuations in the laser cavity length.^{106,108,109,124} Although self-referencing is a useful method for measuring changes in f_0 , practical implementations have some complexities that include the requirement of an octave-spanning bandwidth, perfect mode-matching of the $2\nu_N$ and ν_{2N} modes, and strict temperature control.¹²⁵ Impressive levels of timing jitter and phase noise control have been achieved in recent laboratory experiments,¹²³ which have shown that it is possible to operate an MLL with an MDEV of 3×10^{-19} at $\tau = 10^3 \text{ s}$.¹²⁴

C. SWaP optimization with integrated photonics

A satellite-based implementation of MLL will require significant miniaturization and space-hardening from their current form. A key challenge would be to ensure that there is no degradation in performance as a result—toward this, the field of integrated photonic is paving a potential pathway. In a recent review by Chang *et al.*,⁹⁵ integrated photonic is discussed as an emerging field of development for producing high-volume, low-cost, and SWaP-efficient photonic hardware based on common materials such as silicon (which is widely available).¹²⁶

Current technological directions are focused on replacing individual optical components with their equivalent integrated photonic-solutions one component at a time and testing these devices on a working laboratory setup. For example, Carlson *et al.*¹²⁷ developed an integrated photonic circuit based on silicon nitride that uses multiple waveguides, which are all excited by a single (externally generated) MLL pump. The waveguides produce super-continuum light (spectral-broadened) at wavelengths that corresponded to different optical clock standards. The super-continuum light overlaps with lasers locked to various optical clocks, and heterodyne measurements are conducted to estimate the TDEV between all clocks using the waveguide output. This particular integrated photonic device replaces a bulky spectrum widening apparatus with a low-SWaP chip-based solution. The performance metric achieved includes a residual FFI of 3.8×10^{-15} at $\tau = 2$ s,¹²⁷ which is progress in the right direction. Another study by Jankowski *et al.*¹²⁸ consists of both a photonic chip-based second harmonic generation stage and a chip-based spectral broadening stage were demonstrated. These chip-based devices showed power efficiencies as they consumed order femtojoules of energy—a reduction of 3 orders of magnitudes from previous laboratory-based setups. As the technology of integrated photonic continues to mature, similar SWaP optimizations could be expected for all the various components used in clock synchronization.^{95,98,129}

D. Experiments in space

To our knowledge, there have recently been three space-based experiments that have demonstrated the operation of MLL-based frequency combs in space. Although these experiments used a single spacecraft (satellite or sounding rocket), the findings shed some insights on the key challenges and opportunities that lay ahead as the field transitions to large-scale network of free-space MLL links (as shown in Fig. 1). In a recent mission in collaboration between the Korean Advanced Institute of Science and Technology and the South Korean Satellite Technology Research Center, an erbium fiber (Er:fiber) MLL was tested onboard the satellite STSAT-2C.¹³⁰ This particular MLL emitted pulses with $T_0 = 350$ fs, an $f_r = 25$ MHz, and was centered at a 1590 nm wavelength. During the mission, the MLL successfully endured the high-accelerations during launch^{134,135} as well as high-energy space-radiation¹³⁶ with limited changes to the MLL parameters. Lee *et al.*¹³⁰ showed that the MLL could sustain continuous operation over one year and, for instance, achieve an f_r FFI of 10^{-12} at $\tau = 10$ s¹³⁷ throughout the year. This performance was despite an 8.6% reduction in the average MLL output power level, which is attributed to radiation-induced attenuation. For a complete description of the setup, please see Ref. 130; we briefly highlight that the comb stabilization setup included a saturable absorber (for

passive mode-locking that was directly inserted to avoid using bulk optics) and a ring-type piezoelectric actuator system (to stabilize f_r). As future recommendations, some hardware suggestions were made, including the use of an active temperature control unit for greater noise reduction and thicker aluminum shielding for radiation proofing. Although these suggestions would increase the overall SWaP, the use of integrated photonic could provide alternative options.

In the FOKUS I mission, a substantially shorter experiment was conducted with the sounding rockets that lasted 360 s in total.¹³¹ An Er:fiber MLL was again used, but this time to continuously compare the TDEV between an optical and microwave clock. In particular, MLL was phase-locked to the 384 THz optical transitions of a rubidium optical clock and then compared to the transitions of a cesium atomic clock that oscillates at 10 MHz via the f_r and f_0 frequency comb parameters. The performance achieved during the operation was an FFI of 10^{-11} at $\tau = 20$ s;¹³¹ however, the experimental duration was too short for any further meaningful conclusions. A successive mission, the FOKUS II, took the lessons learnt from FOKUS I and used a testing payload with lower SWaP than the FOKUS I.¹³¹ Furthermore, a dual-comb setup was used with two MLLs to compare TDEV between an iodine-based optical clock at 281 THz optical transition and a cesium atomic clock. The FOKUS II achieved an ADEV of 4×10^{-12} at $\tau = 100$ s.¹³¹ Although, since the FFI method used in the FOKUS I mission was not made clear, we cannot easily compare the performance between both missions. Nevertheless, as an early demonstration, both the FOKUS I and II missions show that MLLs can be used to autonomously and continuously compare between different clock technologies in space, while sustaining reasonably low levels of FFI.

A final space-based experiment that is currently under development is by Takeuchi *et al.*¹³³ The setup proposed in this experiment also uses an Er:fiber MLL placed in the shape of the number eight with a nonlinear polarization rotation device used for stabilization. Early ground-based tests conducted continuously over several days are showing stable operation with FFI of 10^{-14} at $\tau = 2000$ s.¹³³ A summary of all satellite-based experiments is presented in Table II. Due to the limited standardization in the field currently, some entries are missing—as the field matures in coming years, we encourage reporting of these metrics for greater ease of assessment of space-readiness.

E. Optical two-way time and frequency transfer

The most prominent MLL-based clock synchronization technique is O-TWTFT. First proposed by Giorgetta *et al.*,¹² O-TWTFT combines the lessons learned from fiber-based time-frequency transfer^{138–141} and the microwave-based two-way time-frequency transfer.⁶⁶ In O-TWTFT, two sets of MLL pulses are locally produced and phase-locked to two different clocks. These MLL pulses are then exchanged over free space in a two-way configuration and compared via an interferometric method such as linear optical sampling.¹⁰⁴ Through interferometry, the time-of-flight or phase differences between the two sets of pulses are compared, which corresponds to the degree to which the two clocks are out of sync. A series of experiments over progressively longer free-space terrestrial links have been conducted using O-TWTFT in recent

TABLE II. Comparison of recent satellite-based experiments and proposals using MLL-based frequency combs. The aim of this table is to suggest similarities between certain attributes and also point out some parameters that are often missing in the literature, but are crucial for an assessment of space-readiness. It should be noted that the symbols in the following include P_{in} : the input pump power and P_{out} : the output seed power.

Project (Year)	Technology	Pump (nm)	Seed (nm)	f_r (MHz)	T_0 (fs)	P_{in} (mW)	P_{out} (mW)	Volume (L)	Weight (kg)
STSAT-2C ¹³⁰ (2014)	Er:fiber	980	1590	25	350	600	14	3.3	2.5
FOKUS I ¹³¹ (2016)	Er:fiber	780	1560	100	...	10	...	15	20
FOKUS II ¹³² (2021)	Er:fiber	980	1560	100	45	...	180	7	10
proposed ¹³³ (2021)	Er:fiber	976	1560	48.7	0.8

times.^{12,13,28,142–144} The results from these experiments and those from some previous fiber-based methods are presented in Table III for ease of comparison.

From Table III, it is clear that there have been a large number of O-TWTFT experiments in recent years. However, the experiments conducted from 2013 to 2021 had limited free-space range (i.e., less than 30 km). A key obstacle in these experiments has been the linear optical sampling method and, in particular, the relatively high signal strength (order nanowatts) required for optimal photodetection, which is a key part of conventional linear optical sampling. Some technical strategies were proposed to overcome this issue, which have focused on meeting the power demand by increasing the transmit power, using a larger receiver telescope aperture, or using an adaptive optics setup.²⁸ However, these methods all add to the SWaP costs of the overall setup and would thus have limited prospects in space.

Fortunately, a SWaP-friendly direction has been recently developed that focuses instead on improving the linear optical sampling method by using something called a time programmable frequency comb (TPFC).^{15–17,45} The TPFC is a highly precise MLL that can be tuned in time and phase in a coherent manner with sub-10 as accuracy.^{15,16} In traditional linear optical sampling,^{12–14,104,135,144} a signal MLL is sampled using another “local” MLL using heterodyne detection. Instead of a local MLL, a TPFC can be used to provide finer-tuning capabilities during sampling. Using a TPFC

greatly improves the accuracy of measurements and has been shown to enable reductions in the required receiver power level from nanowatts to order 0.1 pW.¹⁷

Over a 300 km terrestrial link, the TPFC-based O-TWTFT was used to synchronize two distant clocks to a best-case TDEV of 500 as, which was at the SQL for this particular setup.¹⁷ The achievable MDEV was 3×10^{-19} at $\tau = 10^3$ s.¹⁷ This performance is near the state of the art considering that the free-space link experienced 102 dB loss and the median received signal power level was only 0.15 pW.¹⁷ Moreover, the TPFC was not pre-amplified at the transmitter, and this performance level was achieved without adaptive optics. Notably, Caldwell *et al.*¹⁷ also demonstrated a Kalman filter to continuously monitor the TDEV between the local and signal MLL during the absence of deep fades.

In summary, there are some promising directions that have been laid for clock synchronization using classical frequency combs. Recent developments in the field have demonstrated that using optical signals, instead of microwave, allows for achieving a lower FFI with shorter τ , which are essential for satellite-based optical clock synchronization. Furthermore, using a pulsed signal rather than CW offers a more robust method against turbulent channels. A TPFC-based system also enables a longer link with limited additional complex hardware and would be a SWaP-friendlier option. Furthermore, the TPFC method is able to reach the SQL in performance and thus may be a good solution for satellite-based deployment in

TABLE III. Recent field experiments using MLL-based classical frequency combs over optical fiber and terrestrial links and their reported performance metrics. The general trend across the recent free-space experiments has been toward longer link range, shorter integration time (τ), and an MDEV below 10^{-18} (in turn, lower TDEV).

Author	Year	Protocol	Link type	Nodes	Path (km)	MDEV	Integration time, τ (s)	TDEV (s)
Predehl <i>et al.</i> ¹³⁸	2012	OFT	Fiber	11	920	10^{-18}	10^3	6×10^{-16}
Droste <i>et al.</i> ¹³⁹	2013	OFT	Fiber	2	1840	4×10^{-19}	10^2	2×10^{-17}
Bercy <i>et al.</i> ¹⁴⁰	2014	OFT	Fiber	2	100	5×10^{-21}	10^3	3×10^{-18}
Giorgetta <i>et al.</i> ¹²	2013	O-TWTFT	Free-space	2	2	10^{-18}	10^3	6×10^{-16}
Deschenes <i>et al.</i> ¹³	2016	O-TWTFT	Free-space	2	4	5×10^{-19}	10^4	3×10^{-15}
Sinclair <i>et al.</i> ¹⁴³	2018	O-TWTFT	Free-space	2	4	10^{-17}	1	7×10^{-18}
Sinclair <i>et al.</i> ¹⁴⁵	2019	O-TWTFT	Free-space	2	4	10^{-18}	10^2	6×10^{-17}
Bodine <i>et al.</i> ¹⁴⁵	2020	O-TWTFT	Free-space	3	14	10^{-18}	10^2	6×10^{-17}
Ellis <i>et al.</i> ¹⁴	2021	O-TWTFT	Free-space	3	28	10^{-18}	2×10^2	1×10^{-16}
Shen <i>et al.</i> ²⁸	2022	O-TWTFT	Free-space	2	113	4×10^{-19}	10^4	2×10^{-15}
Caldwell <i>et al.</i> ¹⁷	2023	O-TWTFT	Free-space	2	300	5×10^{-18}	1×10^3	3×10^{-16}

the future. In our perspective, integrated photonic will also play a key role toward space-readiness and aid in the miniaturization of key optical components. However, sustaining the precise stabilization and noise suppression performance of current laboratory setups in these future space-ready solutions will be a challenge.

IV. QUANTUM FREQUENCY COMBS

In this section, we provide details on the potential advantage (i.e., quantum advantage) of using a quantum frequency comb instead of a classical frequency comb as the signal in clock synchronization. We show how quantum frequency combs are generated from classical frequency combs, the unique properties that quantum-based techniques exploit, the advantage in theory, and the main challenges for a free-space implementation of quantum-enhanced clock synchronization.

A. Generating quantum frequency combs

Let us begin with an outline of common methods for generating quantum frequency combs. The generation stage of a quantum frequency comb strictly requires an optical non-linearity, such as a $\chi^{(2)}$ or $\chi^{(3)}$ process. Both nonlinear processes typically have low generation efficiency and, as a result, quantum frequency combs generally have low output power than classical frequency combs although, as discussed further in this section, certain strategies can be used to improve the generation efficiency. In this work, we focus on $\chi^{(2)}$ and its implementation in spontaneous parametric downconversion (SPDC).

The $\chi^{(2)}$ non-linearity can be induced using nonlinear crystals, such as BBO (beta barium borate), LBO (lithium triborate), KTP (potassium titanyl phosphate), or BIBO (BiB₃O₆).^{21,146–149} When an MLL-based classical frequency comb is used as the input pump, the classical frequency comb will convert into a quantum frequency comb after passing through the crystal and undergoing a process known as SPDC. The conversion process can be from a single-pass through the crystal or after multiple passes when the crystal is placed inside a resonant cavity.^{146,150,151} In principle, SPDC consists of converting a “pump” into a “signal” and an “idler.”

When the pump is a monochromatic CW laser centered at frequency ν_p , the SPDC output is a monochromatic CW signal at frequency ν_s and a monochromatic CW idler at ν_i , such that

$$\nu_p = \nu_s + \nu_i \quad \text{and} \quad \vec{k}_p = \vec{k}_s + \vec{k}_i, \quad (13)$$

where $\vec{k}_{p,s,i}$ are the momentum vectors of the pump, signal, and idler respectively. The SPDC is considered fully degenerate when the signal and idler are indistinguishable in terms of their center frequency, direction of travel, and polarization, i.e., $\nu_s = \nu_i = \nu_p/2$. Fully degenerate operation is desired as this induces phase-sensitive variance in the signal and idler quadratures, where the variance is reduced below the SQL at a certain phase—a phenomenon known as quadrature-squeezing.^{152,153} However, fully degenerate SPDC is challenging to achieve in practice and strongly depends on factors such as the pump power and crystal temperature conditions.¹⁵⁴ Single-pass SPDC also suffers from low efficiency since a large portion of the pump photons usually pass through the crystal unconverted.¹⁵⁵ In Fig. 7, we have shown how single-pass SPDC is used to produce quadrature-squeezed states.

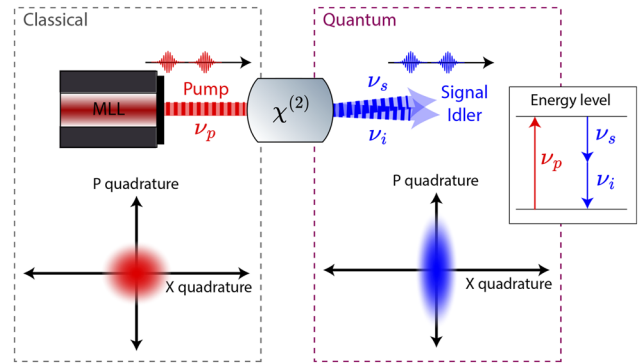


FIG. 7. Spontaneous parametric downconversion (SPDC) process is a $\chi^{(2)}$ non-linear process that can be used to convert a classical frequency comb (e.g., mode-locked laser, MLL) into a quantum frequency comb that exhibits quadrature-squeezing properties. The implementation of SPDC shown above is degenerate whereby the signal and idler have exactly half the energy (in turn center frequency) as the pump. As an example, we show the phase space diagram of the classical and quantum frequency comb with X-quadrature-squeezing. Evidently, the quantum frequency comb has reduced variance in the X quadrature and would correspondingly yield a more precise measurement than the classical frequency comb.

Let us take a brief aside to define the term “quadrature.” Quadrature refers to the quantum-version of the real and imaginary components of an electromagnetic wave.¹⁵⁶ For instance, an electric-field amplitude, $E(\vec{r}, t)$, with spatial coordinate vector \vec{r} and time coordinate t is given by¹⁵⁶

$$E(\vec{r}, t) \propto X(\vec{r}, t) \cos(2\pi\nu_0 t) + iP(\vec{r}, t) \sin(2\pi\nu_0 t), \quad (14)$$

where $X(\vec{r}, t)$ and $P(\vec{r}, t)$ are the quadrature amplitudes with real numbers. In the quantum perspective, the quadratures are unit-less operators with an expectation and standard deviation, which we denote in this work as simple X and P , respectively. A quadrature-squeezed quantum state has a variance in one quadrature that is below the SQL, and in the other quadrature, the variance is above the SQL,¹⁵³ as shown in Fig. 7.

Returning to SPDC, improving the efficiency of single-pass SPDC is crucial for producing a useful quantum frequency comb. Two main strategies in the literature include using a pulsed pump, such as an MLL instead of a CW pump, and placing the crystal inside a resonant cavity.^{157–163} An MLL has a higher peak power relative to an equivalent CW laser, which considerably improves the conversion efficiency. Furthermore, a resonant cavity builds up energy with each pass further increasing the peak power. The optical parametric oscillator (OPO) is a parametric oscillator that satisfies both efficiency strategies. A version of the OPO tailored for a pumped laser system is called the synchronously pumped optical parametric oscillator (SPOPO). The SPOPO uses a cavity that has a precisely controlled length that is locked to the pumping MLL’s f_p (and, in turn, the round-trip time of a single pulse). The state-of-the-art conversion efficiency of a SPOPO system is currently at ~20%.¹⁶⁴ For fully degenerate SPDC within the SPOPO, the MLL pump must have a peak power that is below (but as close as possible to) the oscillation threshold of the cavity. Operating near the cavity threshold also helps maximize the quadrature-squeezing level produced in the

output.¹⁵⁸ A visual diagram of a typical SPOPO setup with a second harmonic generator and an OPO is shown in Fig. 10.

An MLL has a broadband spectrum with a large number of frequency modes (in practice around 10^5 modes¹⁵⁹) as described by Eq. (12). Each of these frequency modes will down-convert during SPDC following Eq. (13) and produce a considerably more complex signal and idler than in the monochromatic CW case. Particularly, in the fully degenerate case, both signal and idler will span an identical range of frequency modes $\nu_s = \nu_i = (Nf_r + f_0)/2$ that exhibits multi-partite entanglement between the frequency modes.¹⁴⁷ For the purpose of clock synchronization, we are instead interested in an alternative (simpler) description of the “complex” signal and idler state, which can be achieved via a unitary change in the basis.^{146,147,150,159} In particular, the eigenmodes of the SPOPO, which are constructed by taking a linear combination over all frequency modes, gives a new basis in which each the signal and idler can be characterized by the outgoing pulse spectral amplitude and phase profiles.¹⁵⁹ In the eigenmode basis, quadrature-squeezing is observed when the MLL pump has a peak power below the cavity threshold. Visualizations of the X-quadrature-squeezed quantum frequency comb generated by a SPOPO are shown in Figs. 7 and 10.

Quantum frequency combs with quadrature-entanglement can also be produced using the SPOPO method. In this case, two quadrature-squeezed quantum frequency combs would be mixed on a 50 : 50 beam splitter. Before the mixing, it will be important to ensure that the two quantum frequency combs exhibit squeezing in different quadratures, which can be achieved by applying a path delay in one of the paths equivalent to a $\pi/2$ phase delay. The two output signals from the beam splitter would exhibit variance below the SQL in the sum and difference quadrature modes—thus the quadratures are entangled. This particular configuration for producing quadrature-entanglement has been implemented¹⁶⁵ and is shown in Fig. 8.

While SPOPOs have been used widely in many laboratory experiments, key issues exist when we consider extending the

technique to space. Most notably, miniaturizing the SPOPO cavity while sustaining high-efficiency and high-bandwidth in the output has proven to be a challenging task to date.^{166–168} In a recent study by Stokowski *et al.*,¹⁶⁹ a new technique was developed, which demonstrates an operating OPO on a small-form integrated device based on thin-film lithium niobate. The conversion efficiency achieved on this device was $\sim 34\%$, which is at the current state of the art. More pathways to achieving OPO on integrated photonic devices are required as the field evolves further and will be a key road block for quantum frequency combs on satellites.

Finally, we note that the Kerr non-linearity is yet another technique for producing quantum frequency combs. The Kerr non-linearity gives rise to a $\chi^{(3)}$ process called four-wave mixing (FWM). In FWM, two or three input frequencies are converted into two or one output frequencies, respectively, via a parametric process that conserves energy. Recently, FWM has been used to generate a specific type of quantum frequency comb using a CW laser pump, which exhibits quadrature-squeezing and quadrature-entanglement properties in individual frequency modes.^{137,170–177} These quantum frequency combs, also referred to as “Kerr optical frequency combs,” may provide a new method for quantum-enhanced clock synchronization. We note, however, due to our current focus on quantum frequency combs that exhibit quadrature-squeezing and quadrature-entanglement over a basis that spans over all frequency modes (i.e., the output of a SPOPO), Kerr optical frequency combs are beyond the scope of our study.

B. Optimal clock synchronization

The main objective of quantum-enhanced clock synchronization is to extend the performance of classical clock synchronization from the SQL toward the HL. A quantum frequency comb is one key tool to this end, as discussed further in Sec. IV B 2. However, in addition, we also need an “optimal” measurement strategy. Although the linear optical sampling technique is currently a popu-

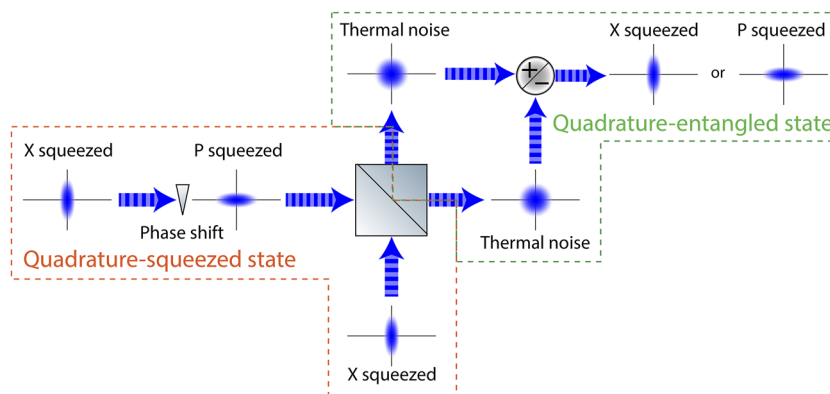


FIG. 8. Method for producing a quadrature-entangled quantum frequency comb by mixing two quadrature-squeezed states onto a 50 : 50 beam splitter.^{23,153,165} The two inputs must be quadrature-squeezed in orthogonal quadratures, and this can be achieved (for example) by using a $\pi/2$ phase shifting stage on one of the input arms. After a sum/difference stage, the final output will exhibit quadrature-squeezing. In a recent study,²³ we compared the performance of a quadrature-entangled state against a quadrature-squeezed state²² for inter-satellite quantum-enhanced clock synchronization.

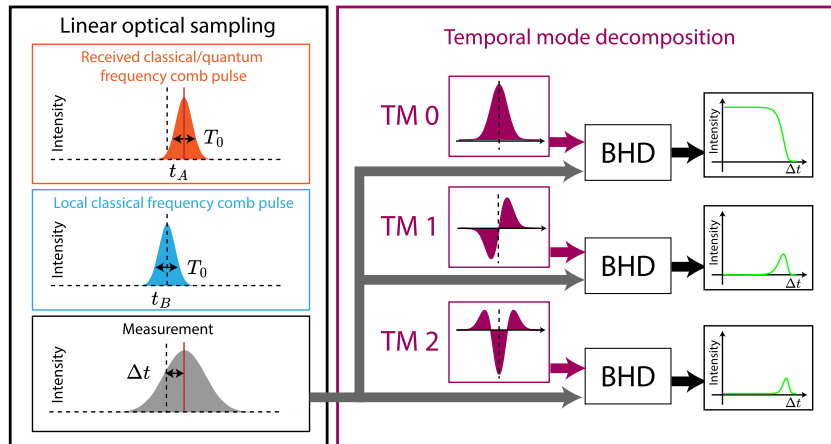


FIG. 9. Linear optical sampling method as used in O-TWTFT consists of estimating the timing offset, Δt , between two classical frequency combs (i.e., $\Delta t = t_A - t_B$) using interferometry. On the right, we show an optimal measurement strategy—temporal mode decomposition, where the linear optical sampling measurement is projected onto higher-order temporal modes before the temporal modes are separately measured. The photocurrent outputs of each temporal mode measurement ℓ is proportional to $(\Delta t)^\ell$ with a standard deviation of Δt measurements given by Eq. (17). Substituting the classical frequency comb with a quantum frequency comb as the signal would yield a standard deviation scaling that approaches the HL given by Eq. (18). It should be noted that BHD represents balanced homodyne detection and TM represents temporal mode. A temporal mode decomposition setup could, in principle, comprise of an infinite number of temporal modes, although only the first three temporal modes are show above.

lar method for estimating the timing offset (i.e., Δt in Fig. 9) between two classical frequency combs, it is not the optimal measurement strategy according to quantum estimation theory.^{20,158} One example of an optimal measurement strategy for estimating Δt is a technique that we refer to here as “temporal mode decomposition.” In temporal mode decomposition, the combined signal from the received (classical or quantum) frequency comb and local classical frequency comb is projected onto higher-order orthogonal temporal modes and the intensity of each temporal mode is measured separately, as shown in Fig. 9 and discussed in previous studies.^{20,158,178–180} A classical frequency comb signal with temporal mode decomposition can reach the SQL.²⁰ A quantum frequency comb signal with temporal mode decomposition will exceed the SQL and approach the HL.

1. Reaching the SQL with temporal mode decomposition

In an experiment implementing clock synchronization, several samples of Δt are collected to calculate the average timing offset, $\bar{\Delta t}$, and corresponding standard deviation, $\sigma_{\Delta t}$. It should be noted that $\sigma_{\Delta t}$ and TDEV are related, where the former is a statistical standard deviation of Δt and the latter is the average two-sample deviation of Δt (discussed in Sec. II A). Ideally, we want $\sigma_{\Delta t} \rightarrow 0$ by averaging over a large number of samples of Δt ; however, experimental challenges such as restrictions to the transmit power, channel-based losses, and detection inefficiencies limit the number of samples that can be collected in practice. In addition, different clock synchronization strategies can achieve different $\sigma_{\Delta t}$ over a finite number of samples over the same link. Hence, finding a measurement strategy that minimizes $\sigma_{\Delta t}$ (i.e., an optimal measurement strategy) is desired.

Measurement strategies that use time-of-flight, such as linear optical sampling, have a measurement standard deviation that scales with the total number of photons collected (n) given by²⁰

$$\sigma_{\Delta t, \text{time-of-flight}} \propto \frac{T_0}{\sqrt{n}} \tag{15}$$

Here, minimizing T_0 (with ultra-short duration pulses) and maximizing n are the only two strategies for minimizing the standard deviation. Alternatively, measurement strategies based on the phase difference between a remote and local signal, $\Delta\phi$, [which is, in turn, related to $\Delta t := \Delta\phi/(2\pi\nu_0)$] include OFT. The phase method has a standard deviation that scales as²⁰

$$\sigma_{\Delta t, \text{phase}} \propto \frac{1}{\nu_0 \sqrt{n}}, \tag{16}$$

where ν_0 , recall, is the nominal frequency of the signal. Finally, the temporal mode decomposition method provides a superior scaling of the standard deviation compared to both the time-of-flight and phase measurements, which is given by^{20,158}

$$\sigma_{\Delta t, \text{TM}} \propto \frac{1}{\sqrt{n((1/T_0)^2 + \nu_0^2)}}, \tag{17}$$

where TM denotes temporal modes. The difference in the standard deviation here is due to the fact that the temporal modes of a quantum frequency comb pulse carry both the time-of-flight and the phase information in their temporal profiles. In addition, temporal mode decomposition has also been shown to be an *optimal* measurement strategy according to quantum estimation theory,¹⁵⁸ and therefore, Eq. (17) represents the lowest bound in the standard

deviation achievable by any measurement strategy when a classical frequency comb signal is used.

2. Reaching the HL with a quantum frequency comb

There remains one final strategy that can be used to lower $\sigma_{\Delta t}$ further and that is to substitute the classical frequency comb signal with a quantum frequency comb signal. A quantum frequency comb with quadrature squeezing of factor r would retrieve a standard deviation that scales as²⁰

$$\sigma_{\Delta t, TM} \propto \frac{\exp(-r)}{\sqrt{n((1/T_0)^2 + v_0^2)}} \rightarrow \frac{1}{n\sqrt{(1/T_0)^2 + v_0^2}}, \quad (18)$$

where the right-hand side is reached as $r \rightarrow \infty$; see Ref. 183 for specific details on the derivation. Therefore, using a quantum frequency comb and temporal mode decomposition allows us to reach the HL, i.e., $\sigma_{\Delta t} \propto 1/n$.

Initial studies by Giovanneti *et al.*^{78–81} inspired research into quantum-enhanced clock synchronization. Recently, a proposal by Lamine *et al.*²⁰ discussed a practical pathway toward achieving the HL using a quantum frequency comb and a balanced homodyne detection setup. In the proposal by Lamine *et al.*,²⁰ a quadrature-squeezed quantum frequency comb is recommended as the signal. A second classical frequency comb is recommended as the local oscillator at the remote site. To perform temporal mode decomposition in this setup, balanced homodyne detection is used. Before balanced homodyne detection takes place, however, the local oscillator first passes through a pulse shaper to modify the signal-envelope into the shape of the second temporal mode.^{20,21,151,162} This “shaped” local oscillator is then mixed with the incoming quantum frequency comb on a beam splitter, which projects the signal onto the second-order temporal mode. The final output after balanced homodyne detection is a photocurrent with an intensity that is proportional to Δt . This particular setup is shown in Fig. 10. In Fig. 9, we show how temporal mode decomposition could be used to simultaneously measure multiple higher-order temporal modes.

In Fig. 10, we show a diagram of a free-space experimental setup for the proposed scheme by Lamine *et al.*,²⁰ which we have investigated in our previous studies.^{22,23} The local quantum frequency comb is transmitted over free space to the remote site, where the two frequency combs are mixed on a 50 : 50 beam splitter that is part of the balanced homodyne detection setup. The balanced homodyne detection setup projects the incoming signal onto the temporal modes of the remote classical frequency comb and extracts an electrical signal that is proportional to Δt . After several samples are collected, $\sigma_{\Delta t}$ will scale as per Eq. (18).

In a laboratory experiment, Wang *et al.*²¹ successfully conducted temporal mode decomposition to achieve $\sigma_{\Delta t, TM}$ as per Eq. (18) with a 1.5 dB quadrature-squeezed quantum frequency comb. The setup consisted of a Ti:sapphire-based MLL that generated (ultra-short) 130 fs duration pulses with $v_0 = 0.25$ THz and $f_r = 75$ MHz. The remote classical frequency comb was produced using the same MLL source. The 1.5 dB of quadrature-squeezing was achieved using an SPOPO setup,^{150,158,159} which successfully reduced the $\sigma_{\Delta t}$ from 8.9×10^{-23} to 7.5×10^{-23} s. These laboratory results confirm that temporal mode decomposition can be conducted in practice to yield quantum advantage. To aid in gaining an intuitive understanding of the result, Fig. 11 shows the difference between the expected measurement results using a quantum vs a classical frequency comb as the signal with temporal mode decomposition. Based on the signal-to-noise ratio, it can be deduced that the quantum approach would be able to resolve weaker signal levels and thereby provide precision enhancements for clock synchronization.

C. Challenges to achieving quantum advantage in practice

The results by Wang *et al.*²¹ have inspired our recent work on satellite-based quantum-enhanced clock synchronization in LEO.^{22,23} Our work has revealed some opportunities as well as challenges for the temporal mode decomposition method and, in turn, achieving quantum advantage in practice. Particularly, we

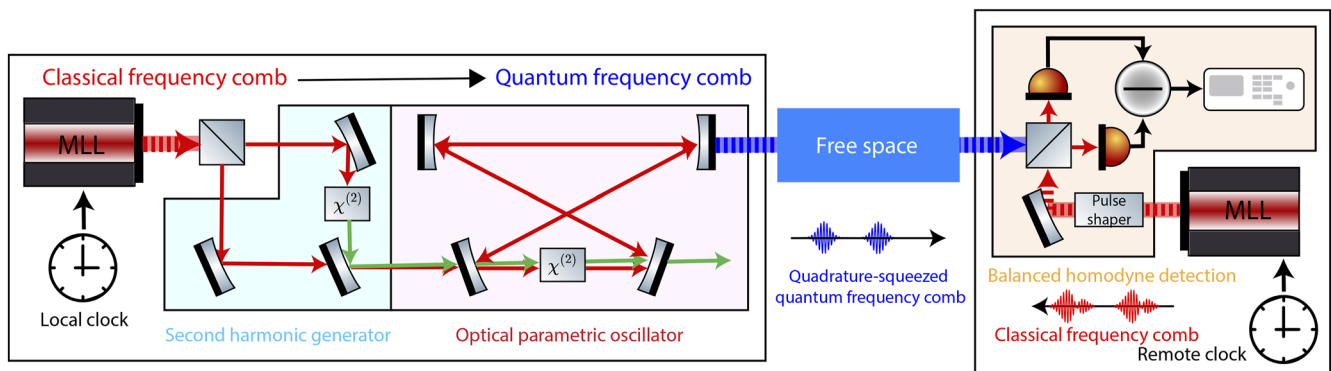


FIG. 10. Potential setup for quantum-enhanced clock synchronization using the scheme proposed by Lamine *et al.*²⁰ An MLL phase-locked to a local optical clock is quadrature-squeezed via a second harmonic generator and optical parametric oscillator setup before being transmitted over free-space to a remote site. At the remote site, a second MLL is temporally shaped to a specific superposition of higher-order temporal mode before mixing with the incoming signal. Balanced homodyne detection produces an electronic photocurrent that is proportional to the temporal offset, Δt , between local and remote frequency comb pulses (and in turn the difference between the local and remote clocks).

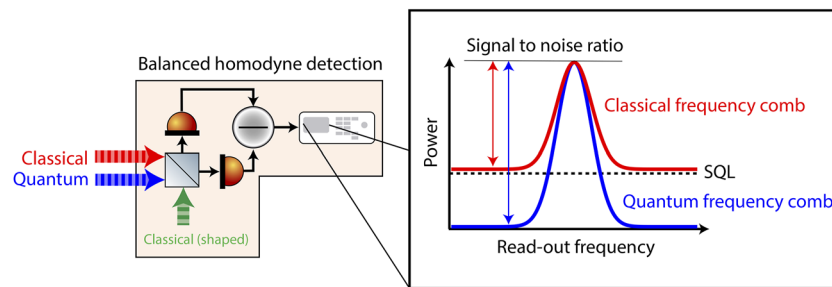


FIG. 11. Expected advantage of using a quantum frequency comb relative to a classical frequency comb in clock synchronization over a balanced homodyne detection setup. Red indicated the classical frequency comb, which has a noise floor at the SQL. Blue indicates the quantum frequency comb that would have a reduced noise floor proportional to the level of quadrature-squeezing. Hence, the quantum approach shows a pathway to achieving a higher signal-to-noise ratio by reducing the noise floor. It should be noted that quantum advantage has been experimentally demonstrated by Wang *et al.*²¹

have found that that quantum advantage is highly sensitive to beam diffraction, satellite pointing misalignment, and photodetection inefficiencies. In addition, differences between the generation efficiency of classical vs quantum frequency combs impact the level of n captured in practice and, in turn, the $\sigma_{\Delta t}$ achievable. The practical realization of quantum advantage thereby relies on three important factors: (1) the efficient generation of quantum frequency combs, (2) the minimal impact of noise and loss during free-space propagation, and (3) the near-perfect detection of the quantum frequency comb at the remote site.

Precision beyond the SQL, toward the HL, relies strongly on the ability to generate *useful* quantum properties of light. Unfortunately, current state-of-the-art laboratory methods for generating quantum frequency combs have low efficiencies—in some state-of-the-art laboratory setups, the overall conversion efficiency is as low as 10%.¹⁸² On the other hand, state-of-the-art studies with classical frequency combs have demonstrated conversion efficiencies reaching 50% and better.⁹⁵ Based on this difference alone, for n quantum frequency comb photons vs n classical frequency comb photons, a $>5\times$ reduction of $\sigma_{\Delta t}$ would be required at a minimum to justify deploying the quantum approach. In terms of the equivalent quadrature-squeezing level, this equates to a requirement of >7 dB of quadrature squeezing,¹⁸⁶ which is near the state of the art. For this reason, in coming years more research focus is required in improving the efficiency of generating quadrature-squeezed quantum frequency combs.

However, we must emphasize that conversion efficiencies are seldom reported in the literature, and we encourage greater transparency in this regard. The values reported here represent frequency combs with wavelengths spanning a 12.1 nm bandwidth between ~ 1277 – 1289 nm for the quantum case¹⁸² and an 8 nm bandwidth between ~ 1554 – 1564 nm for the classical case.⁹⁵ Based on Eq. (18), quantum frequency combs with wide bandwidth and shorter wavelengths (higher ν_0) are desired; however, these properties need to be traded-off with susceptibility to loss over the free-space channel.

Quadrature-squeezing and quadrature-entanglement properties are also highly sensitive to photonic loss and noise issues. In our work,^{22,23} we found that beam diffraction and satellite pointing issues contribute as loss and noise, respectively, to a quantum

frequency comb.^{22,23} While the noise contributions due to satellite pointing could be controlled by using fine-tracking control systems for real-time tracking of satellites and ground stations on-board,^{184–187} photonic loss over the channel due to beam diffraction and turbulence is unfortunately irrecoverable. To compensate for the consequent degradation of quantum properties, we could use “stronger” quantum properties (i.e., higher squeezing level) or sophisticated loss compensation techniques^{85,188} with noiseless amplification¹⁸⁹ and degenerate parametric amplification^{189–191} at the remote receiver. These techniques have not yet been studied in the context of quantum-enhanced clock synchronization and are open directions of much-needed research.

Finally, the photodetectors (inside the balanced homodyne detection setup) can also contribute loss and noise to the quantum frequency comb if they have photodetection efficiency less than 100%.²² Fortunately, state-of-the-art photodetection efficiencies, achieved in laboratory settings, have been of order 90% and greater.^{85,111} A recent experiment with positive-intrinsic-negative photodetectors reached 99.5% efficiency and, as a result, could measure 15 dB of quadrature squeezing of a CW laser with a center wavelength of 1064 nm.¹⁶¹ In the near future, we expect similar levels of performance on-board satellites; however, achieving 90% photodetection efficiency on chip-based platforms (with low SWaP demand) is yet another on-going challenge in the field.¹⁹² Recent work on super-conducting nanowire-based balanced homodyne detection setups have demonstrated successful operation, with 77% photodetection efficiency in a low size and weight packaging.¹⁹³ These super-conducting photodetectors were able to measure the quadrature variance of a CW laser with center wavelength at 1550 nm. However, it is predicted that the current photodetection efficiency of 77% would limit the measurement of squeezing to 6.3 dB.¹⁹³ In addition, super-conducting devices require cryogenics, which add to the overall SWaP demand. Implementation of balanced homodyne detection in space is yet another open field of research.

In our recent study, we found that at least 15 dB of quadrature squeezing is required to achieve $2\times$ quantum advantage over a typical 100 km inter-satellite link that consists of LEO satellites with telescopic apertures of 0.3 m radius (0.6 m diameter) and photodetectors operating at 90% efficiency.²² Unfortunately, 15 dB quadrature squeezing is at the current state-of-the-art,¹⁶¹

and even higher squeezing levels would dramatically increase the SWaP demand of the system. In addition, we found that the satellite pointing angle jitter of both the local and the remote satellites needs to be within a standard deviation of $1 \mu\text{rad}$. If the standard deviation is above this level, the consequential degradation would eliminate any quantum advantage. Hence, a significant engineering effort is required for inter-satellite transfer of quadrature-squeezed quantum frequency combs. Finally, we found that photonic loss due to beam diffraction limits the range of the inter-satellite links to within 300 km. For longer-range inter-satellite links, unfortunately multiple LEO satellites would be needed in a “multi-hop” configuration.

D. Quadrature-squeezing vs quadrature-entanglement over free space

Although quadrature squeezing has largely been the focus of our discussion, quadrature-entanglement could, in principle, be used instead to yield a squeezed variance, as discussed in Sec. IV A and shown in Fig. 8. Our study on quadrature squeezing has revealed certain system characteristics that are required in order to achieving quantum advantage over inter-satellite links.²² In particular, quadrature-entanglement provides an alternative quantum property that could be exploited to achieve the HL. However, it is important to note that, in principle, the scaling of $\sigma_{\Delta t}$ using a quadrature-entangled quantum frequency comb is the exact same as quadrature squeezing, as shown by us in a previous study.²³ In other words, the resulting signal-to-noise ratio gain achieved by using a quadrature-entangled quantum frequency comb would be the same as a quadrature-squeezed comb of equivalent r . Instead, the advantage of a quadrature-entanglement is in the greater resilience this state provides over lossy free-space channels. Particularly, the quadrature-correlations shared between pairs of quadrature-entangled quantum frequency comb pulses can be taken advantage of to recover over asymmetrically lossy channels.²³ Asymmetric loss is expected over dynamically varying channels, such as inter-satellite and ground-satellite links, hence in these contexts, quadrature-entanglement may be a better solution than quadrature squeezing.

Finally, we mention that no previous experimental studies have been conducted on the propagation of quantum frequency combs over turbulent atmospheric channels. Hence, little is known about the impact of turbulence on quadrature squeezing and quadrature entanglement over these types of free-space channels. In 2014, Peuntinger *et al.*¹⁹⁴ investigated the transfer of polarization squeezing using a CW laser (not from a quantum frequency comb) over a 1.6 km free-space channel. Their study found that the polarization degree of freedom offers some level of resilience against the turbulence-induced phase and waveform distortions. This insight may transfer to future experiments with quantum frequency combs.

V. PERSPECTIVE AND OUTLOOK

Both classical and quantum frequency combs can be used for satellite-based clock synchronization of a network of optical clocks. MLLs are a highly stable source of classical frequency combs, and it has already been demonstrated, within laboratory settings,

that state-of-the-art MLL stabilization and noise suppression levels exceed the requirements to synchronize optical clocks. Furthermore, recent experiments with MLLs in space have provided valuable insights into some of the key engineering strategies required to develop MLLs that can withstand launch acceleration and radiation. In addition, developments in the field of integrated photonics will enable chip-based MLL generation in the coming years. MLLs can synchronize distant clocks over a 300 km terrestrial link with O-TWTFT and achieve an FFI and TDEV near the SQL. On the other hand, quantum frequency combs, generated by converting an MLL-based classical frequency comb through a SPOPO, can also exhibit the superior stabilization and noise suppression performance of MLLs with added quantum properties. By combining an optimal measurement strategy (e.g., temporal mode decomposition) with a quantum frequency comb signal, the HL can be approached. Since satellites have strict SWaP restrictions, physically realizing performance at the HL will enable much-needed resource efficiencies.

Classical frequency combs are more mature in terms of technical readiness than quantum frequency combs. In our perspective, O-TWTFT could be deployed over satellite-ground and inter-satellite links in the near future. However, future implementations of the linear optical sampling method should include temporal mode decomposition for optimal measurement. This step will maximize the precision achievable by linear optical sampling. Although further research is required to better understand the performance of the temporal mode decomposition method over channels with atmospheric turbulence and Doppler shifts, it is also our perspective that T2L2 could be improved with temporal mode decomposition and balanced homodyne detection with “slow” photodetector sampling rates in the microwave region. There may also be scenarios such as on-board low-powered platforms including CubeSats, where T2L2 is preferred over O-TWTFT due to less “complex” hardware.

The key road-block for quantum frequency combs is the relatively low efficiency with which they can be generated at present. The generation efficiency needs to be improved to a level that is comparable with the generation efficiency of classical frequency combs. In addition, we want to encourage more transparency on the conversion efficiency values for various quantum frequency comb-generation methods proposed in the literature. A second limitation on quantum frequency combs is the sensitivity to photonic losses and noise. We recommend research effort toward the development of mitigation strategies at the receiver (or transmitter) for enabling the free-space propagation of quadrature-squeezing and quadrature-entanglement over realistic link distances.

As a final note, we also mention that there are many fields of research that would benefit from performance near the HL. These applications include spectroscopy,^{195–197} chemistry,¹⁹⁸ gravitational wave detection,^{199,200} communications,²⁰¹ ranging,¹⁵ and angle estimation.²⁰² As an illustrative example we mention that, in a recent experiment, a classical frequency comb was used to estimate range down to an uncertainty in distance of 10 nm using only 10 nW of received power and over a $\tau = 40 \mu\text{s}$ window.¹⁵ Had a quantum frequency comb been used instead, the uncertainty in distance could have been as low as 4 pm (i.e., 4 orders of magnitude smaller) for the

same received power level and τ .²⁰³ Although, this quantum advantage would be in the most ideal case with infinite squeezing, any finite levels of squeezing can produce orders of magnitude enhancements, providing between 1 and 4 orders of magnitudes overall. Similar gains could also be expected in future space-borne gravitational wave detectors, where a reduction in the laser phase noise below the SQL during arm locking could substantially improve the sensitivity of the apparatus.²⁰⁰

VI. CONCLUSION

In this perspective on the field of satellite-based synchronization, we have reviewed the current state-of-the-art in timing and synchronization, emphasizing the need for an optical-frequency based approach. Furthermore, we have outlined the performance characteristics of various optical schemes based on recent experiments conducted over terrestrial links, highlighting the key advantages offered by a frequency-comb based scheme.

We have described how the classical frequency comb is robust, highly stable, and a high-precision solution with certain SWaP advantages over other classical methods. Recent experiments with classical frequency combs have shown successful operation over turbulent channels, while satellite-based experiments have sustained mode-locking capabilities in space over year-long missions. Although inter-satellite, ground-to-satellite, and satellite-to-ground tests are yet to be conducted, the current state-of-the-art shows promise for successful operation in these settings as well. However, new challenges do lie ahead, including overcoming the effect of Doppler shifts during satellite motion.

We have also described how a quantum frequency comb has the potential to provide precision-to-resource advantages that go beyond the capabilities of a classical frequency comb. In resource-constrained environments, such as satellite networks, we have outlined how the quantum approach would, in principle, be a better solution than the equivalent classical approach due to the ability to reach the HL during clock synchronization. However, some limiting factors exist with regard to practical implementations, including the generation efficiency and the fragility of squeezing and entanglement over free space.

There are many open questions in relation to the use of classical and quantum frequency combs for satellite-based clock synchronization. In terms of technological readiness, we have discussed how classical frequency combs have reached higher maturity and, as such, future research efforts on their use should focus on reducing the SWaP footprint and conducting experiments over satellite-based links on the path to commercialization. With regard to quantum frequency combs, we have highlighted that higher-efficiency generation of quantum states is a key road-block at present to further progress and that better understanding of the mechanisms for overcoming the effects of loss and noise over free-space links are required.

ACKNOWLEDGMENTS

R.K.G. is supported by an Australian Government Research Training Program Scholarship and the Sydney Quantum Academy. Approved for Public Release: NG24-1117.

AUTHOR DECLARATIONS

Conflict of Interest

The authors have no conflicts to disclose.

Author Contributions

R.K.G. led the conception of the manuscript, wrote the structure, original draft, and final manuscript. R.M. reviewed the structure, original draft and final manuscript, and supervised the project. H.L., R.A., J.G., and P.B. reviewed the structure, original draft and final manuscript. All authors read and approved the final manuscript.

Ronakraj K. Gosalia: Conceptualization (lead); Formal analysis (lead); Investigation (lead); Methodology (lead); Validation (lead); Writing – original draft (lead); Writing – review & editing (lead). **Ryan Aguinardo:** Conceptualization (equal); Investigation (equal); Validation (equal); Writing – review & editing (equal). **Jonathan Green:** Conceptualization (equal); Investigation (equal); Validation (equal); Writing – review & editing (equal). **Holly Leopardi:** Conceptualization (equal); Methodology (equal); Validation (equal); Writing – review & editing (equal). **Peter Breerton:** Conceptualization (equal); Investigation (equal); Validation (equal); Writing – review & editing (equal). **Robert Malaney:** Conceptualization (equal); Formal analysis (equal); Methodology (equal); Project administration (lead); Supervision (lead); Validation (equal); Writing – review & editing (equal).

DATA AVAILABILITY

The data that support the findings of this study are available from the corresponding author upon reasonable request.

REFERENCES

- A. D. Ludlow, T. Zelevinsky, G. K. Campbell, S. Blatt, M. M. Boyd, M. H. G. de Miranda, M. J. Martin, J. W. Thomsen, S. M. Foreman, J. Ye, T. M. Fortier, J. E. Stalnaker, S. A. Diddams, Y. Le Coq, Z. W. Barber, N. Poli, N. D. Lemke, K. M. Beck, and C. W. Oates, "Sr lattice clock at 1×10^{-16} fractional uncertainty by remote optical evaluation with a Ca clock," *Science* **319**, 1805–1808 (2008).
- N. Poli, C. W. Oates, P. Gill, and G. M. Tino, "Optical atomic clocks," *Riv. Nuovo Cimento* **36**, 555–624 (2013); [arXiv:1407.3493](https://arxiv.org/abs/1407.3493).
- H. Katori, "Optical lattice clocks and quantum metrology," *Nat. Photonics* **5**, 203–210 (2011).
- C. Clivati, R. Ambrosini, T. Artz, A. Bertarini, C. Bortolotti, M. Frittelli, F. Levi, A. Mura, G. Maccaferri, M. Nanni, M. Negusini, F. Perini, M. Roma, M. Stagni, M. Zucco, and D. Calonico, "A VLBI experiment using a remote atomic clock via a coherent fibre link," *Sci. Rep.* **7**, 40992 (2017).
- T. E. Mehlstäubler, G. Grosche, C. Lisdat, P. O. Schmidt, and H. Denker, "Atomic clocks for geodesy," *Rep. Prog. Phys.* **81**, 064401 (2018); [arXiv:1803.01585](https://arxiv.org/abs/1803.01585).
- E. Boldbaatar, D. Grant, S. Choy, S. Zaminpardaz, and L. Holden, "Evaluating optical clock performance for GNSS positioning," *Sensors* **23**, 5998 (2023).
- A. Derevianko, K. Gibble, L. Hollberg, N. R. Newbury, C. Oates, M. S. Safronova, L. C. Sinclair, and N. Yu, "Fundamental physics with a state-of-the-art optical clock in space," *Quantum Sci. Technol.* **7**, 044002 (2022); [arXiv:2112.10817](https://arxiv.org/abs/2112.10817).
- S. Johannessen, "Time synchronization in a local area network," *IEEE Control Syst. Mag.* **24**, 61–69 (2004).
- D. Krummacker, C. Fischer, K. Alam, M. Karrenbauer, S. Melnyk, H. Dieter Schotten, P. Chen, and S. Tang, "Intra-network clock synchronization for wireless networks: From state of the art systems to an improved solution," in *2020 2nd*

International Conference on Computer Communication and the Internet (IEEE, 2020), pp. 36–44.

- ¹⁰R. N. Gore, E. Lisova, J. Akerberg, and M. Bjorkman, “Clock synchronization in future industrial networks: Applications, challenges, and directions,” in *2020 AET International Annual Conference* (IEEE, 2020), pp. 1–6.
- ¹¹O. Seijo, I. Val, M. Luvisotto, and Z. Pang, “Clock synchronization for wireless time-sensitive networking: A march from microsecond to nanosecond,” *IEEE Ind. Electron. Mag.* **16**, 35–43 (2022).
- ¹²F. R. Giorgetta, W. C. Swann, L. C. Sinclair, E. Baumann, I. Coddington, and N. R. Newbury, “Optical two-way time and frequency transfer over free space,” *Nat. Photonics* **7**, 434–438 (2013).
- ¹³J. D. Deschênes, L. C. Sinclair, F. R. Giorgetta, W. C. Swann, E. Baumann, H. Bergeron, M. Cermak, I. Coddington, and N. R. Newbury, “Synchronization of distant optical clocks at the femtosecond level,” *Phys. Rev. X* **6**, 021016 (2016).
- ¹⁴J. L. Ellis, M. I. Bodine, W. C. Swann, S. A. Stevenson, E. D. Caldwell, L. C. Sinclair, N. R. Newbury, and J.-D. Deschênes, “Scaling up frequency-comb-based optical time transfer to long terrestrial distances,” *Phys. Rev. Appl.* **15**, 034002 (2021).
- ¹⁵E. D. Caldwell, L. C. Sinclair, N. R. Newbury, and J.-D. Deschenes, “The time-programmable frequency comb and its use in quantum-limited ranging,” *Nature* **610**, 667–673 (2022).
- ¹⁶E. D. Caldwell, L. C. Sinclair, N. R. Newbury, and J.-D. Deschênes, “Time programmable frequency comb,” in *Conference on Lasers and Electro-Optics* (Optica Publishing Group, Washington, DC, 2022), pp. 1–2.
- ¹⁷E. D. Caldwell, J.-D. Deschenes, J. Ellis, W. C. Swann, B. K. Stuhl, H. Bergeron, N. R. Newbury, and L. C. Sinclair, “Quantum-limited optical time transfer for future geosynchronous links,” *Nature* **618**, 721–726 (2023); [arXiv:2212.12541](#).
- ¹⁸M. de Burgh and S. D. Bartlett, “Quantum methods for clock synchronization: Beating the standard quantum limit without entanglement,” *Phys. Rev. A* **72**, 042301 (2005); [arXiv:0505112](#) [quant-ph].
- ¹⁹P. Kómár, E. M. Kessler, M. Bishof, L. Jiang, A. S. Sørensen, J. Ye, and M. D. Lukin, “A quantum network of clocks,” *Nat. Phys.* **10**, 582–587 (2014); [arXiv:1310.6045](#).
- ²⁰B. Lamine, C. Fabre, and N. Treps, “Quantum improvement of time transfer between remote clocks,” *Phys. Rev. Lett.* **101**, 123601 (2008); [arXiv:0804.1203](#).
- ²¹S. Wang, X. Xiang, N. Treps, C. Fabre, T. Liu, S. Zhang, and R. Dong, “Sub-shot-noise interferometric timing measurement with a squeezed frequency comb,” *Phys. Rev. A* **98**, 053821 (2018); [arXiv:1802.08384](#).
- ²²R. Gosalia, R. Malaney, R. Aguinaldo, J. Green, and M. Clampin, “Beyond the standard quantum limit in the synchronization of low-earth-orbit satellites,” in *2022 IEEE Latin-American Conference on Communications (LATINCOM)* (IEEE, 2022), pp. 1–6.
- ²³R. Gosalia, R. Malaney, R. Aguinaldo, J. Green, and P. Brereton, “LEO clock synchronization with entangled light,” in *GLOBECOM 2023 - 2023 IEEE Global Communications Conference* (IEEE, 2023), pp. 2317–2322; [arXiv:2305.19639](#).
- ²⁴K. Djerroud, E. Samain, A. Clairon, O. Acef, N. Man, P. Lemonde, and P. Wolf, “A coherent optical link through the turbulent atmosphere,” in *EFTF-2010 24th European Frequency and Time Forum* (IEEE, 2010), Vol. 35, pp. 1–6.
- ²⁵E. Samain, P. Exertier, C. Courde, P. Fridelance, P. Guillemot, M. Laas-Bourez, and J. M. Torre, “Time transfer by laser link: A complete analysis of the uncertainty budget,” *Metrologia* **52**, 423–432 (2015).
- ²⁶G. D. Rovera, M. Abgrall, C. Courde, P. Exertier, P. Fridelance, P. Guillemot, M. Laas-Bourez, N. Martin, E. Samain, R. Sherwood, J. M. Torre, and P. Urich, “A direct comparison between two independently calibrated time transfer techniques: T2L2 and GPS common-views,” *J. Phys.: Conf. Ser.* **723**, 012037 (2016).
- ²⁷D. R. Gozzard, S. W. Schediwy, B. Stone, M. Messineo, and M. Tobar, “Stabilized free-space optical frequency transfer,” *Phys. Rev. Appl.* **10**, 024046 (2018); [arXiv:1806.00945](#).
- ²⁸Q. Shen, J.-Y. Guan, J.-G. Ren, T. Zeng, L. Hou, M. Li, Y. Cao, J.-J. Han, M.-Z. Lian, Y.-W. Chen, X.-X. Peng, S.-M. Wang, D.-Y. Zhu, X.-P. Shi, Z.-G. Wang, Y. Li, W.-Y. Liu, G.-S. Pan, Y. Wang, Z.-H. Li, J.-C. Wu, Y.-Y. Zhang, F.-X. Chen, C.-Y. Lu, S.-K. Liao, J. Yin, J.-J. Jia, C.-Z. Peng, H.-F. Jiang, Q. Zhang, and J.-W. Pan, “Free-space dissemination of time and frequency with 10^{-19} instability over 113 km,” *Nature* **610**, 661–666 (2022).
- ²⁹S. Raupach and G. Grosche, “Chirped frequency transfer: A tool for synchronization and time transfer,” *IEEE Trans. Ultrason. Ferroelectrics Freq. Control* **61**, 920–929 (2014).
- ³⁰R. Jozsa, D. S. Abrams, J. P. Dowling, and C. P. Williams, “Quantum clock synchronization based on shared prior entanglement,” *Phys. Rev. Lett.* **85**, 2010–2013 (2000); [arXiv:1401.8075](#).
- ³¹E. O. Ilo-Okeke, L. Tessler, J. P. Dowling, and T. Byrnes, “Remote quantum clock synchronization without synchronized clocks,” *npj Quantum Inf.* **4**, 40 (2018); [arXiv:1709.08423](#).
- ³²E. O. Ilo-Okeke, L. Tessler, J. P. Dowling, and T. Byrnes, “Entanglement-based quantum clock synchronization,” *AIP Conf. Proc.* **2241**, 020011 (2020).
- ³³H. Dai, Q. Shen, C.-Z. Wang, S.-L. Li, W.-Y. Liu, W.-Q. Cai, S.-K. Liao, J.-G. Ren, J. Yin, Y.-A. Chen, Q. Zhang, F. Xu, C.-Z. Peng, and J.-W. Pan, “Towards satellite-based quantum-secure time transfer,” *Nat. Phys.* **16**, 848–852 (2020); [arXiv:2006.00666](#).
- ³⁴C. Spiess, S. Töpfer, S. Sharma, A. Kržič, M. Cabrejo-Ponce, U. Chandrasekara, N. L. Döll, D. Rieländer, and F. Steinlechner, “Clock synchronization with correlated photons,” *Phys. Rev. Appl.* **19**, 054082 (2023); [arXiv:2108.13466](#).
- ³⁵R. Lafler and R. N. Lanning, “Quantum time transfer: A practical method for lossy and noisy channels,” *Phys. Rev. Appl.* **20**, 024064 (2023); [arXiv:2211.00737](#).
- ³⁶S. Haldar, I. Agullo, A. J. Brady, A. Lamas-Linares, W. C. Proctor, and J. E. Troupe, “Global time distribution via satellite-based sources of entangled photons,” *Phys. Rev. A* **107**, 022615 (2023); [arXiv:2209.15071](#).
- ³⁷C. Spiess and F. Steinlechner, “Clock synchronization with pulsed single photon sources,” *Quantum Sci. Technol.* **9**, 015019 (2024); [arXiv:2212.12589](#).
- ³⁸H. J. Kang, J. Yang, B. J. Chun, H. Jang, B. S. Kim, Y. J. Kim, and S. W. Kim, “Free-space transfer of comb-rooted optical frequencies over an 18 km open-air link,” *Nat. Commun.* **10**, 4438 (2019).
- ³⁹M. Kues, C. Reimer, J. M. Lukens, W. J. Munro, A. M. Weiner, D. J. Moss, and R. Morandotti, “Quantum optical microcombs,” *Nat. Photonics* **13**, 170–179 (2019).
- ⁴⁰IEEE Ultrasonics Ferroelectrics and Frequency Control Society, *IEEE Standard Definitions of Physical Quantities for Fundamental Frequency and Time Metrology—Random Instabilities* (IEEE, 2022).
- ⁴¹W. J. Riley and D. Howe, *Handbook of Frequency Stability Analysis* (NIST, 2008).
- ⁴²E. Rubiola and F. Vernotte, “The companion of Enrico’s chart for phase noise and two-sample variances,” *IEEE Trans. Microwave Theory Tech.* **71**, 2996–3025 (2023); [arXiv:2201.07109](#).
- ⁴³S. S. Nande, M. Paul, S. Senk, M. Ulbricht, R. Bassoli, F. H. Fitzek, and H. Boche, “Quantum enhanced time synchronisation for communication network,” *Comput. Networks* **229**, 109772 (2023).
- ⁴⁴D. W. Allan, “Should the classical variance be used as a basic measure in standards metrology?,” *IEEE Trans. Instrum. Meas.* **IM-36**, 646–654 (1987).
- ⁴⁵E. D. Caldwell, L. C. Sinclair, J. D. Deschenes, F. Giorgetta, and N. R. Newbury, “Application of quantum-limited optical time transfer to space-based optical clock comparisons and coherent networks,” *APL Photonics* **9**, 016112 (2024).
- ⁴⁶S. Zhang, Y. Xiao, P. Yang, Y. Liu, W. Chang, and S. Zhou, “An effectiveness evaluation model for satellite observation and data-downlink scheduling considering weather uncertainties,” *Remote Sens.* **11**, 1621 (2019).
- ⁴⁷S. M. Brewer, J.-S. Chen, A. M. Hankin, E. R. Clements, C. W. Chou, D. J. Wineland, D. B. Hume, and D. R. Leibrandt, “An $^{27}\text{Al}^+$ quantum-logic clock with a systematic uncertainty below 10^{-18} ,” *Phys. Rev. Lett.* **123**, 033201 (2019); [arXiv:1902.07694](#).
- ⁴⁸N. Huntemann, C. Sanner, B. Lipphardt, C. Tamm, and E. Peik, “Single-ion atomic clock with 3×10^{-18} systematic uncertainty,” *Phys. Rev. Lett.* **116**, 063001 (2016); [arXiv:1602.03908](#).
- ⁴⁹B. Jian, J. Bernard, M. Gertsvolf, and P. Dubé, “Improved absolute frequency measurement of the strontium ion clock using a GPS link to the SI second,” *Metrologia* **60**, 015007 (2023).
- ⁵⁰T. Bothwell, D. Kedar, E. Oelker, J. M. Robinson, S. L. Bromley, W. L. Tew, J. Ye, and C. J. Kennedy, “JILA Sr optical lattice clock with uncertainty of 2.0×10^{-18} ,” *Metrologia* **56**, 065004 (2019); [arXiv:1906.06004](#).
- ⁵¹T. L. Nicholson, S. L. Campbell, R. B. Hutson, G. E. Marti, B. J. Bloom, R. L. McNally, W. Zhang, M. D. Barrett, M. S. Safronova, G. F. Strouse, W. L. Tew, and J. Ye, “Systematic evaluation of an atomic clock at 2×10^{-18} total uncertainty,” *Nat. Commun.* **6**, 6896 (2015).

- ⁵²W. F. McGrew, X. Zhang, R. J. Fasano, S. A. Schäffer, K. Beloy, D. Nicolodi, R. C. Brown, N. Hinkley, G. Milani, M. Schioppo, T. H. Yoon, and A. D. Ludlow, "Atomic clock performance enabling geodesy below the centimetre level," *Nature* **564**, 87–90 (2018).
- ⁵³F. Riehle, "Optical clock networks," *Nat. Photonics* **11**, 25–31 (2017).
- ⁵⁴T. A. Ely, E. A. Burt, J. D. Prestage, J. M. Seubert, and R. L. Tjoelker, "Using the deep space atomic clock for navigation and science," *IEEE Trans. Ultrason. Ferroelectrics Freq. Control* **65**, 950–961 (2018).
- ⁵⁵E. A. Burt, J. D. Prestage, R. L. Tjoelker, D. G. Enzer, D. Kuang, D. W. Murphy, D. E. Robison, J. M. Seubert, R. T. Wang, and T. A. Ely, "Demonstration of a trapped-ion atomic clock in space," *Nature* **595**, 43–47 (2021).
- ⁵⁶J. Seubert, T. A. Ely, and J. Stuart, "Results of the deep space atomic clock deep space navigation analog experiment," *J. Spacecr. Rockets* **59**, 1914–1925 (2022).
- ⁵⁷L. Cacciapuoti and C. Salomon, "Space clocks and fundamental tests: The ACES experiment," *Eur. Phys. J.: Spec. Top.* **172**, 57–68 (2009).
- ⁵⁸F. Meynadier, P. Delva, C. le Poncin-Lafitte, C. Guerlin, and P. Wolf, "Atomic clock ensemble in space (ACES) data analysis," *Classical Quantum Gravity* **35**, 035018 (2018); [arXiv:1709.06491](https://arxiv.org/abs/1709.06491).
- ⁵⁹T. Schuldt, K. Abich, T. Alam, J. Bischof, T. Blomberg, L. Blümel, A. Boac, A. Bußmeier, M. Gohlke, F. Kuschewski, M. Oswald, J. Wüst, T. Zechel, X. Amigues, A. Eckardt, W. Halle, B. Zender, J. Hrabina, J. Oulehla, A. Bawamia, K. Döringshoff, C. Kürbis, M. Krutzik, A. Wicht, S. Oschker, M. Jentsch, S. Schweikle, C. Speidel, N. Beller, C. Dahl, M. Großmann, T. Liebherr, K. Voss, and C. Braxmaier, "In-orbit verification of an optical frequency reference on the ISS Bartolomeo platform," *Proc. SPIE* **12777**, 127772A (2023).
- ⁶⁰L. Liu, D. S. Lü, W. B. Chen, T. Li, Q. Z. Qu, B. Wang, L. Li, W. Ren, Z. R. Dong, J. B. Zhao, W. B. Xia, X. Zhao, J. W. Ji, M. F. Ye, Y. G. Sun, Y. Y. Yao, D. Song, Z. G. Liang, S. J. Hu, D. H. Yu, X. Hou, W. Shi, H. G. Zang, J. F. Xiang, X. K. Peng, and Y. Z. Wang, "In-orbit operation of an atomic clock based on laser-cooled ⁸⁷Rb atoms," *Nat. Commun.* **9**, 2760 (2018).
- ⁶¹D. Kirchner, "Two-way time transfer via communication satellites," *Proc. IEEE* **79**, 983–990 (1991).
- ⁶²D. Kirchner, H. Ressler, P. Grudler, F. Baumont, C. Veillet, W. Lewandowski, W. Hanson, W. Klepczynski, and P. Urich, "Comparison of GPS common-view and two-way satellite time transfer over a baseline of 800 km," *Metrologia* **30**, 183–192 (1993).
- ⁶³M. Fujieda, D. Piester, T. Gotoh, J. Becker, M. Aida, and A. Bauch, "Carrier-phase two-way satellite frequency transfer over a very long baseline," *Metrologia* **51**, 253–262 (2014); [arXiv:1403.3193](https://arxiv.org/abs/1403.3193).
- ⁶⁴S. Droste, C. Grebing, J. Leute, S. M. Raupach, A. Matveev, T. W. Hänsch, A. Bauch, R. Holzwarth, and G. Grosche, "Characterization of a 450 km baseline GPS carrier-phase link using an optical fiber link," *New J. Phys.* **17**, 083044 (2015).
- ⁶⁵H. Hachisu, M. Fujieda, S. Nagano, T. Gotoh, A. Nogami, T. Ido, S. Falke, N. Huntemann, C. Grebing, B. Lipphardt, C. Lisdat, and D. Piester, "Direct comparison of optical lattice clocks with an intercontinental baseline of 9000 km," *Opt. Lett.* **39**, 4072 (2014); [arXiv:1403.6285](https://arxiv.org/abs/1403.6285).
- ⁶⁶A. Bauch, "Time and frequency comparisons using radiofrequency signals from satellites," *C. R. Phys.* **16**, 471–479 (2015).
- ⁶⁷W. Schäfer and T. Feldmann, "Perspectives of time and frequency transfer via satellite," *J. Phys.: Conf. Ser.* **723**, 012038 (2016).
- ⁶⁸D. R. Gozzard, L. A. Howard, B. P. Dix-Matthews, S. F. Karpathakis, C. T. Gravestock, and S. W. Schediwy, "Ultra-stable free-space laser links for a global network of optical atomic clocks," *Phys. Rev. Lett.* **128**, 020801 (2022); [arXiv:2103.12909](https://arxiv.org/abs/2103.12909).
- ⁶⁹Q. Shen, J.-Y. Guan, T. Zeng, Q.-M. Lu, L. Huang, Y. Cao, J.-P. Chen, T.-Q. Tao, J.-C. Wu, L. Hou, S.-K. Liao, J.-G. Ren, J. Yin, J.-J. Jia, H.-F. Jiang, C.-Z. Peng, Q. Zhang, and J.-W. Pan, "Experimental simulation of time and frequency transfer via an optical satellite-ground link at 10⁻¹⁸ instability," *Optica* **8**, 471 (2021).
- ⁷⁰B. P. Dix-Matthews, "Coherent optical transmission through atmospheric turbulence," Ph.D. thesis, The University of Western Australia, 2021.
- ⁷¹É. Samain, J. Weick, P. Vrancken, F. Para, D. Albanese, J. Paris, J.-M. Torre, C. Zhao, P. Guillemot, and I. Petitbon, "Time transfer by laser link – The T2L2 experiment on Jason-2 and further experiments," *Int. J. Mod. Phys. D* **17**, 1043–1054 (2008).
- ⁷²E. Samain, G. D. Rovera, J.-M. Torre, C. Courde, A. Belli, P. Exertier, P. Urich, P. Guillemot, R. Sherwood, X. Dong, X. Han, Z. Zhang, W. Meng, and Z. Zhang, "Time transfer by laser link (T2L2) in noncommon view between Europe and China," *IEEE Trans. Ultrason. Ferroelectrics Freq. Control* **65**, 927–933 (2018).
- ⁷³C. Robert, J. M. Conan, and P. Wolf, "Impact of turbulence on high-precision ground-satellite frequency transfer with two-way coherent optical links," *Phys. Rev. A* **93**, 033860 (2016).
- ⁷⁴J. Levine, "A review of time and frequency transfer methods," *Metrologia* **45**, S162 (2008).
- ⁷⁵D. Hanson, "Fundamentals of two-way time transfers by satellite," in *Proceedings of the 43rd Annual Symposium on Frequency Control* (IEEE, 1989), pp. 174–178.
- ⁷⁶A. Belmonte, M. T. Taylor, L. Hollberg, and J. M. Kahn, "Effect of atmospheric anisoplanatism on earth-to-satellite time transfer over laser communication links," *Opt. Express* **25**, 15676 (2017).
- ⁷⁷W. C. Swann, M. I. Bodine, I. Khader, J. D. Deschênes, E. Baumann, L. C. Sinclair, and N. R. Newbury, "Measurement of the impact of turbulence anisoplanatism on precision free-space optical time transfer," *Phys. Rev. A* **99**, 023855 (2019); [arXiv:1811.10989](https://arxiv.org/abs/1811.10989).
- ⁷⁸V. Giovannetti, S. Lloyd, and L. Maccone, "Quantum-enhanced positioning and clock synchronization," *Nature* **412**, 417–419 (2001); [arXiv:0103006](https://arxiv.org/abs/0103006) [quant-ph].
- ⁷⁹V. Giovannetti, S. Lloyd, and L. Maccone, "Positioning and clock synchronization through entanglement," *Phys. Rev. A* **65**, 022309 (2002); [arXiv:0107140](https://arxiv.org/abs/0107140) [quant-ph].
- ⁸⁰V. Giovannetti, S. Lloyd, and L. Maccone, "Quantum-enhanced measurements: Beating the standard quantum limit," *Science* **306**, 1330–1336 (2004).
- ⁸¹V. Giovannetti, S. Lloyd, and L. MacCone, "Advances in quantum metrology," *Nat. Photonics* **5**, 222–229 (2011); [arXiv:1102.2318](https://arxiv.org/abs/1102.2318).
- ⁸²R. Demkowicz-Dobrzański, J. Kołodyński, and M. Guţă, "The elusive Heisenberg limit in quantum-enhanced metrology," *Nat. Commun.* **3**, 1063 (2012); [arXiv:1201.3940](https://arxiv.org/abs/1201.3940).
- ⁸³M. Napolitano, M. Koschorreck, B. Dubost, N. Behbood, R. J. Sewell, and M. W. Mitchell, "Interaction-based quantum metrology showing scaling beyond the Heisenberg limit," *Nature* **471**, 486–489 (2011); [arXiv:1012.5787](https://arxiv.org/abs/1012.5787).
- ⁸⁴M. Zwiernik, C. A. Pérez-Delgado, and P. Kok, "Ultimate limits to quantum metrology and the meaning of the Heisenberg limit," *Phys. Rev. A* **85**, 042112 (2012); [arXiv:1201.2225](https://arxiv.org/abs/1201.2225).
- ⁸⁵S. Zhou, M. Zhang, J. Preskill, and L. Jiang, "Achieving the Heisenberg limit in quantum metrology using quantum error correction," *Nat. Commun.* **9**, 78 (2018); [arXiv:1706.02445](https://arxiv.org/abs/1706.02445).
- ⁸⁶M. Napolitano, M. Koschorreck, B. Dubost, N. Behbood, R. Sewell, and M. W. Mitchell, "Quantum optics and the 'Heisenberg limit' of measurement," *Opt. Photonics News* **22**, 40 (2011).
- ⁸⁷S. A. Diddams, "The evolving optical frequency comb [Invited]," *J. Opt. Soc. Am. B* **27**, B51 (2010).
- ⁸⁸H. Haus, "Mode-locking of lasers," *IEEE J. Sel. Top. Quantum Electron.* **6**, 1173–1185 (2000).
- ⁸⁹S. T. Cundiff, J. Ye, and J. L. Hall, "Optical frequency synthesis based on mode-locked lasers," *Rev. Sci. Instrum.* **72**, 3749–3771 (2001).
- ⁹⁰S. T. Cundiff and J. Ye, "Colloquium: Femtosecond optical frequency combs," *Rev. Mod. Phys.* **75**, 325–342 (2003).
- ⁹¹J. Jin, "Dimensional metrology using the optical comb of a mode-locked laser," *Meas. Sci. Technol.* **27**, 022001 (2016).
- ⁹²J. Ma, Z. Qin, G. Xie, L. Qian, and D. Tang, "Review of mid-infrared mode-locked laser sources in the 2.0 μm–3.5 μm spectral region," *Appl. Phys. Rev.* **6**, 021317 (2019).
- ⁹³T. Fortier and E. Baumann, "20 years of developments in optical frequency comb technology and applications," *Commun. Phys.* **2**, 153 (2019); [arXiv:1909.05384](https://arxiv.org/abs/1909.05384).
- ⁹⁴S. A. Diddams, K. Vahala, and T. Udem, "Optical frequency combs: Coherently uniting the electromagnetic spectrum," *Science* **369**, eaay3676 (2020).
- ⁹⁵L. Chang, S. Liu, and J. E. Bowers, "Integrated optical frequency comb technologies," *Nat. Photonics* **16**, 95–108 (2022).
- ⁹⁶I. Ricciardi, S. Mosca, M. Parisi, F. Leo, T. Hansson, M. Erkintalo, P. Maddaloni, P. De Natale, S. Wabnitz, and M. De Rosa, "Optical frequency combs in quadratically nonlinear resonators," *Micromachines* **11**, 230 (2020); [arXiv:2004.04714](https://arxiv.org/abs/2004.04714).

- ⁹⁷A. Kovach, D. Chen, J. He, H. Choi, A. H. Dogan, M. Ghasemkhani, H. Taheri, and A. M. Armani, "Emerging material systems for integrated optical Kerr frequency combs," *Adv. Opt. Photonics* **12**, 135–222 (2020).
- ⁹⁸W. Wang, L. Wang, and W. Zhang, "Advances in soliton microcomb generation," *Adv. Photonics* **2**, 034001 (2020).
- ⁹⁹H. Hu and L. K. Oxenløwe, "Chip-based optical frequency combs for high-capacity optical communications," *Nanophotonics* **10**, 1367–1385 (2021).
- ¹⁰⁰P. W. Smith, "Mode-locking of lasers," *Proc. IEEE* **58**, 1342–1357 (1970).
- ¹⁰¹P. W. Smith, M. A. Duguay, and E. P. Ippen, "Mode-locking of lasers," *Prog. Quantum Electron.* **3**, 107–229 (1974).
- ¹⁰²J. L. Hall, "Nobel lecture: Defining and measuring optical frequencies," *Rev. Mod. Phys.* **78**, 1279–1295 (2006).
- ¹⁰³S. Cundiff, T. Fortier, J. Ye, and J. Hall, "Carrier-envelope phase stabilization of femtosecond mode-locked lasers and direct optical frequency synthesis," in *Technical Digest. Summaries of papers presented at the Conference on Lasers and Electro-Optics. Postconference Technical Digest (IEEE Cat. No. 01CH37170)* (IEEE, 2001), Vol. 288, pp. 635–639.
- ¹⁰⁴C. Dorrer, D. Kilper, H. Stuart, G. Raybon, and M. Raymer, "Linear optical sampling," *IEEE Photonics Technol. Lett.* **15**, 1746–1748 (2003).
- ¹⁰⁵J. Kim and Y. Song, "Ultralow-noise mode-locked fiber lasers and frequency combs: Principles, status, and applications," *Adv. Opt. Photonics* **8**, 465–540 (2016).
- ¹⁰⁶H. Tian, Y. Song, and M. Hu, "Noise measurement and reduction in mode-locked lasers: Fundamentals for low-noise optical frequency combs," *Appl. Sci.* **11**, 7650 (2021).
- ¹⁰⁷H. Tian, W. Yang, D. Kwon, R. Li, Y. Zhao, J. Kim, Y. Song, and M. Hu, "Optical frequency comb noise spectra analysis using an asymmetric fiber delay line interferometer," *Opt. Express* **28**, 9232–9243 (2020).
- ¹⁰⁸R. Herda and O. G. Okhotnikov, "Effect of amplified spontaneous emission and absorber mirror recovery time on the dynamics of mode-locked fiber lasers," *Appl. Phys. Lett.* **86**, 011113 (2005).
- ¹⁰⁹R. Liao, C. Mei, Y. Song, A. Demircan, and G. Steinmeyer, "Spontaneous emission noise in mode-locked lasers and frequency combs," *Phys. Rev. A* **102**, 013506 (2020).
- ¹¹⁰J. Mulet and J. Mork, "Analysis of timing jitter in external-cavity mode-locked semiconductor lasers," *IEEE J. Quantum Electron.* **42**, 249–256 (2006).
- ¹¹¹Y. Wang, H. Tian, D. Hou, F. Meng, Y. Ma, H. Xu, F. X. Kärtner, Y. Song, and Z. Zhang, "Timing jitter reduction through relative intensity noise suppression in high-repetition-rate mode-locked fiber lasers," *Opt. Express* **27**, 11273–11280 (2019).
- ¹¹²H. Bao, Y. J. Wen, and H.-F. Liu, "Impact of saturable absorption on performance of optical clock recovery using a mode-locked multisection semiconductor laser," *IEEE J. Quantum Electron.* **40**, 1177–1185 (2004).
- ¹¹³Y. Mao, Z. Lu, J. Liu, P. J. Poole, and G. Liu, "Pulse timing jitter estimated from optical phase noise in mode-locked semiconductor quantum dash lasers," *J. Lightwave Technol.* **38**, 4787–4793 (2020).
- ¹¹⁴Y. Song, C. Kim, K. Jung, H. Kim, and J. Kim, "Timing jitter optimization of mode-locked Yb-fiber lasers toward the attosecond regime," *Opt. Express* **19**, 14518 (2011); [arXiv:1106.0451](https://arxiv.org/abs/1106.0451).
- ¹¹⁵D. Li, A. Benedick, U. Demirbas, A. Sennaroglu, J. G. Fujimoto, and F. X. Kärtner, "Attosecond timing jitter pulse trains from semiconductor saturable absorber mode-locked Cr:LiSAF lasers," in *2012 Conference on Lasers and Electro-Optics (CLEO)* (IEEE, 2012), Vol. 20, pp. 14518–14525.
- ¹¹⁶D. Hou, C.-C. Lee, Z. Yang, and T. R. Schibli, "Timing jitter characterization of mode-locked lasers with <1 zs/√Hz resolution using a simple optical heterodyne technique," *Opt. Lett.* **40**, 2985 (2015).
- ¹¹⁷T. C. Briles, D. C. Yost, A. Cingöz, J. Ye, and T. R. Schibli, "Simple piezoelectric-actuated mirror with 180 kHz servo bandwidth," *Opt. Express* **18**, 9739–9746 (2010).
- ¹¹⁸D. von der Linde, "Characterization of the noise in continuously operating mode-locked lasers," *Appl. Phys. B* **39**, 201–217 (1986).
- ¹¹⁹F. Haberl, M. Ober, M. Hofer, M. Fermann, E. Wintner, and A. Schmidt, "Low-noise operation modes of a passively mode-locked fiber laser," *IEEE Photonics Technol. Lett.* **3**, 1071–1073 (1991).
- ¹²⁰H. Haus and A. Mecozzi, "Noise of mode-locked lasers," *IEEE J. Quantum Electron.* **29**, 983–996 (1993).
- ¹²¹S. Namiki and H. Haus, "Noise of the stretched pulse fiber laser. I. Theory," *IEEE J. Quantum Electron.* **33**, 649–659 (1997).
- ¹²²R. Paschotta, "Noise of mode-locked lasers (Part II): Timing jitter and other fluctuations," *Appl. Phys. B* **79**, 163–173 (2004).
- ¹²³Y. Ma, B. Xu, H. Ishii, F. Meng, Y. Nakajima, I. Matsushima, T. R. Schibli, Z. Zhang, and K. Minoshima, "Low-noise 750 MHz spaced ytterbium fiber frequency combs," *Opt. Lett.* **43**, 4136 (2018).
- ¹²⁴Z. Deng, Y. Liu, Z. Zhu, D. Luo, C. Gu, L. Zhou, G. Xie, and W. Li, "Ultra-precise optical phase-locking approach for ultralow noise frequency comb generation," *Opt. Laser Technol.* **138**, 106906 (2021).
- ¹²⁵M. Endo, T. D. Shoji, and T. R. Schibli, "Ultralow noise optical frequency combs," *IEEE J. Sel. Top. Quantum Electron.* **24**, 1–13 (2018).
- ¹²⁶D. Thomson, A. Zilkie, J. E. Bowers, T. Komljenovic, G. T. Reed, L. Vivien, D. Marris-Morini, E. Cassan, L. Virost, J. M. Fédéli, J. M. Hartmann, J. H. Schmid, D. X. Xu, F. Boeuf, P. O'Brien, G. Z. Mashanovich, and M. Nedeljkovic, "Roadmap on silicon photonics," *J. Opt.* **18**, 073003 (2016).
- ¹²⁷D. R. Carlson, D. D. Hickstein, A. Lind, J. B. Olson, R. W. Fox, R. C. Brown, A. D. Ludlow, Q. Li, D. Westly, H. Leopardi, T. M. Fortier, K. Srinivasan, S. A. Diddams, and S. B. Papp, "Photonic-chip supercontinuum with tailored spectra for counting optical frequencies," *Phys. Rev. Appl.* **8**, 014027 (2017).
- ¹²⁸M. Jankowski, C. Langrock, B. Desiatov, A. Marandi, C. Wang, M. Zhang, C. R. Phillips, M. Lončar, and M. M. Fejer, "Ultrabroadband nonlinear optics in nanophotonic periodically poled lithium niobate waveguides," *Optica* **7**, 40–46 (2020).
- ¹²⁹A. L. Gaeta, M. Lipson, and T. J. Kippenberg, "Photonic-chip-based frequency combs," *Nat. Photonics* **13**, 158–169 (2019).
- ¹³⁰J. Lee, K. Lee, Y. S. Jang, H. Jang, S. Han, S. H. Lee, K. I. Kang, C. W. Lim, Y. J. Kim, and S. W. Kim, "Testing of a femtosecond pulse laser in outer space," *Sci. Rep.* **4**, 5134 (2014).
- ¹³¹M. Lezius, T. Wilken, C. Deutsch, M. Giunta, O. Mandel, A. Thaller, V. Schkolnik, M. Schiemangk, A. Dinkelaker, A. Kohfeldt, A. Wicht, M. Krutzik, A. Peters, O. Hellmig, H. Duncker, K. Sengstock, P. Windpassinger, K. Lampmann, T. Hülsing, T. W. Hänsch, and R. Holzwarth, "Space-borne frequency comb metrology," *Optica* **3**, 1381 (2016).
- ¹³²B. J. Pröbster, M. Lezius, O. Mandel, C. Braxmaier, and R. Holzwarth, "FOKUS II—Space flight of a compact and vacuum compatible dual frequency comb system," *J. Opt. Soc. Am. B* **38**, 932–939 (2021).
- ¹³³Y. Takeuchi, R. Saito, S. Endo, K. Matsusaka, and M. Musha, "Development of an all PM mode lock fiber laser for space borne frequency reference," *Proc. SPIE* **11852**, 1185230 (2021).
- ¹³⁴E. Baumann, F. R. Giorgetta, J. W. Nicholson, W. C. Swann, I. Coddington, and N. R. Newbury, "High-performance, vibration-immune, fiber-laser frequency comb," *Opt. Lett.* **34**, 638–639 (2009).
- ¹³⁵L. C. Sinclair, I. Coddington, W. C. Swann, G. B. Rieker, A. Hati, K. Iwakuni, and N. R. Newbury, "Operation of an optically coherent frequency comb outside the metrology lab," *Opt. Express* **22**, 6996–7006 (2014).
- ¹³⁶B. P. Fox, K. Simmons-Potter, D. A. Kliner, and S. W. Moore, "Effect of low-earth orbit space on radiation-induced absorption in rare-earth-doped optical fibers," *J. Non-Cryst. Solids* **378**, 79–88 (2013).
- ¹³⁷H. Lee, T. Chen, J. Li, K. Y. Yang, S. Jeon, O. Painter, and K. J. Vahala, "Chemically etched ultrahigh-Q wedge-resonator on a silicon chip," *Nat. Photonics* **6**, 369–373 (2012).
- ¹³⁸K. Predehl, G. Grosche, S. M. F. Raupach, S. Droste, O. Terra, J. Alnis, T. Legero, T. W. Hänsch, T. Udem, R. Holzwarth, and H. Schnatz, "A 920-kilometer optical fiber link for frequency metrology at the 19th decimal place," *Science* **336**, 441–444 (2012).
- ¹³⁹S. Droste, F. Ozimek, T. Udem, K. Predehl, T. W. Hänsch, H. Schnatz, G. Grosche, and R. Holzwarth, "Optical-frequency transfer over a single-span 1840 km fiber link," *Phys. Rev. Lett.* **111**, 110801 (2013).
- ¹⁴⁰A. Bercy, F. Stefani, O. Lopez, C. Chardonnet, P.-E. Pottie, and A. Amy-Klein, "Two-way optical frequency comparisons at 5×10^{-21} relative stability over 100-km telecommunication network fibers," *Phys. Rev. A* **90**, 061802 (2014).
- ¹⁴¹B. Ning, S. Y. Zhang, D. Hou, J. T. Wu, Z. B. Li, and J. Y. Zhao, "High-precision distribution of highly stable optical pulse trains with 8.8×10^{-19} instability," *Sci. Rep.* **4**, 5109 (2014).

- ¹⁴²L. C. Sinclair, W. C. Swann, H. Bergeron, E. Baumann, M. Cermak, I. Coddington, J.-D. Deschènes, F. R. Giorgetta, J. C. Juárez, I. Khader, K. G. Petrillo, K. T. Souza, M. L. Dennis, and N. R. Newbury, "Synchronization of clocks through 12 km of strongly turbulent air over a city," *Appl. Phys. Lett.* **109**, 151104 (2016).
- ¹⁴³L. C. Sinclair, H. Bergeron, W. C. Swann, E. Baumann, J. D. Deschènes, and N. R. Newbury, "Comparing optical oscillators across the air to milliradians in phase and 10^{-17} in frequency," *Phys. Rev. Lett.* **120**, 050801 (2018).
- ¹⁴⁴M. I. Bodine, J. L. Ellis, W. C. Swann, S. A. Stevenson, J.-D. Deschènes, E. D. Hannah, P. Manurkar, N. R. Newbury, and L. C. Sinclair, "Optical time-frequency transfer across a free-space, three-node network," *APL Photonics* **5**, 076113 (2020).
- ¹⁴⁵L. C. Sinclair, H. Bergeron, W. C. Swann, I. Khader, K. C. Cossel, M. Cermak, N. R. Newbury, and J.-D. Deschènes, "Femtosecond optical two-way time-frequency transfer in the presence of motion," *Phys. Rev. A* **99**, 023844 (2019); [arXiv:1808.07040](#).
- ¹⁴⁶G. Patera, N. Treps, C. Fabre, and G. J. de Valcárcel, "Quantum theory of synchronously pumped type I optical parametric oscillators: Characterization of the squeezed supermodes," *Eur. Phys. J. D* **56**, 123–140 (2010); [arXiv:0907.4550](#).
- ¹⁴⁷R. Medeiros de Araújo, J. Roslund, Y. Cai, G. Ferrini, C. Fabre, and N. Treps, "Full characterization of a highly multimode entangled state embedded in an optical frequency comb using pulse shaping," *Phys. Rev. A* **89**, 053828 (2014); [arXiv:1401.4867](#).
- ¹⁴⁸Y. Kobayashi, K. Torizuka, A. Marandi, R. L. Byer, R. A. McCracken, Z. Zhang, and D. T. Reid, "Femtosecond optical parametric oscillator frequency combs," *J. Opt.* **17**, 094010 (2015).
- ¹⁴⁹L. La Volpe, S. De, T. Kouadou, D. Horoshko, M. I. Kolobov, C. Fabre, V. Parigi, and N. Treps, "Multimode single-pass spatio-temporal squeezing," *Opt. Express* **28**, 12385–12394 (2020).
- ¹⁵⁰G. J. de Valcárcel, G. Patera, N. Treps, and C. Fabre, "Multimode squeezing of frequency combs," *Phys. Rev. A* **74**, 061801(R) (2007).
- ¹⁵¹G. Patera, "Quantum properties of ultra-short pulses generated by SPOPOs: Multi-mode squeezing and entanglement," Ph.D. thesis (Université Pierre et Marie Curie, 2018).
- ¹⁵²L.-A. Wu, H. J. Kimble, J. L. Hall, and H. Wu, "Generation of squeezed states by parametric down conversion," *Phys. Rev. Lett.* **57**, 2520–2523 (1986).
- ¹⁵³A. I. Lvovsky, "Squeezed light," *Photonics: Sci. Found., Technol. Appl.* **1**, 121–163 (2015); [arXiv:1401.4118](#).
- ¹⁵⁴U. L. Andersen, T. Gehring, C. Marquardt, and G. Leuchs, "30 years of squeezed light generation," *Phys. Scr.* **91**, 053001 (2016); [arXiv:1511.03250](#).
- ¹⁵⁵C. Couteau, "Spontaneous parametric down-conversion," *Contemp. Phys.* **59**, 291–304 (2018); [arXiv:1809.00127](#).
- ¹⁵⁶H. Bachor and T. C. Ralph, in *A Guide to Experiments in Quantum Optics*, 3rd ed. (Wiley, 2019), pp. 24–26, 97–108.
- ¹⁵⁷C. M. Caves, "Quantum-mechanical noise in an interferometer," *Phys. Rev. D* **23**, 1693–1708 (1981).
- ¹⁵⁸S. Jiang, N. Treps, and C. Fabre, "A time/frequency quantum analysis of the light generated by synchronously pumped optical parametric oscillators," *New J. Phys.* **14**, 043006 (2012).
- ¹⁵⁹O. Pinel, P. Jian, R. M. De Araujo, J. Feng, B. Chalopin, C. Fabre, and N. Treps, "Generation and characterization of multimode quantum frequency combs," *Phys. Rev. Lett.* **108**, 083601 (2012); [arXiv:1103.6123](#).
- ¹⁶⁰J. Roslund, R. M. De Araujo, S. Jiang, C. Fabre, and N. Treps, "Wavelength-multiplexed quantum networks with ultrafast frequency combs," *Nat. Photonics* **8**, 109–112 (2014); [arXiv:1307.1216](#).
- ¹⁶¹H. Vahlbruch, M. Mehmet, K. Danzmann, and R. Schnabel, "Detection of 15 dB squeezed states of light and their application for the absolute calibration of photoelectric quantum efficiency," *Phys. Rev. Lett.* **117**, 110801 (2016).
- ¹⁶²C. Fabre and N. Treps, "Modes and states in quantum optics," *Rev. Mod. Phys.* **92**, 035005 (2020); [arXiv:1912.09321](#).
- ¹⁶³W. Yang, W. Diao, C. Cai, T. Wu, K. Wu, Y. Li, C. Li, C. Duan, H. Leng, N. Zi, and X. Yin, "A bright squeezed light source for quantum sensing," *Chemosensors* **11**, 18 (2022).
- ¹⁶⁴M. Gao, N. M. Lüpken, and C. Fallnich, "Highly efficient and widely tunable Si₃N₄ waveguide-based optical parametric oscillator," *Opt. Express* **32**, 10899–10909 (2024).
- ¹⁶⁵T. Eberle, V. Händchen, and R. Schnabel, "Stable control of 10 dB two-mode squeezed vacuum states of light," *Opt. Express* **21**, 11546–11553 (2013); [arXiv:1305.3383](#).
- ¹⁶⁶F. Mondain, T. Lunghi, A. Zavatta, E. Gouzien, F. Doutré, M. de Micheli, S. Tanzilli, and V. D'Auria, "Chip-based squeezing at a telecom wavelength," *Photon. Res.* **7**, A36–A39 (2019).
- ¹⁶⁷A. W. Bruch, X. Liu, J. B. Surya, C.-L. Zou, and H. X. Tang, "On-chip $\chi^{(2)}$ microring optical parametric oscillator," *Optica* **6**, 1361 (2019); [arXiv:1909.07422](#).
- ¹⁶⁸L. Zhang, C. Cui, J. Yan, Y. Guo, J. Wang, and L. Fan, "On-chip parallel processing of quantum frequency comb," *npj Quantum Inf.* **9**, 57 (2023).
- ¹⁶⁹H. S. Stokowski, D. J. Dean, A. Y. Hwang, T. Park, O. T. Celik, T. P. McKenna, M. Jankowski, C. Langrock, V. Ansari, M. M. Fejer, and A. H. Safavi-Naeini, "Integrated frequency-modulated optical parametric oscillator," *Nature* **627**, 95–100 (2024); [arXiv:2307.04200](#).
- ¹⁷⁰P. Del'Haye, A. Schliesser, O. Arcizet, T. Wilken, R. Holzwarth, and T. J. Kippenberg, "Optical frequency comb generation from a monolithic microresonator," *Nature* **450**, 1214–1217 (2007); [arXiv:0708.0611](#).
- ¹⁷¹T. J. Kippenberg, R. Holzwarth, and S. A. Diddams, "Microresonator-based optical frequency combs," *Science* **332**, 555–559 (2011).
- ¹⁷²C. Bao, L. Zhang, A. Matsko, Y. Yan, Z. Zhao, G. Xie, A. M. Agarwal, L. C. Kimerling, J. Michel, L. Maleki, and A. E. Willner, "Nonlinear conversion efficiency in Kerr frequency comb generation," *Opt. Lett.* **39**, 6126 (2014).
- ¹⁷³A. Dutt, K. Luke, S. Manipatruni, A. L. Gaeta, P. Nussenzveig, and M. Lipson, "On-chip optical squeezing," *Phys. Rev. Appl.* **3**, 044005 (2015); [arXiv:1309.6371](#).
- ¹⁷⁴Y. K. Chemo, "Kerr optical frequency combs: Theory, applications and perspectives," *Nanophotonics* **5**, 214–230 (2016).
- ¹⁷⁵Y. K. Chemo, "Quantum dynamics of Kerr optical frequency combs below and above threshold: Spontaneous four-wave mixing, entanglement, and squeezed states of light," *Phys. Rev. A* **93**, 033820 (2016); [arXiv:1412.5700](#).
- ¹⁷⁶A. S. Mayer and B. C. Kirkpatrick, "Silicon photonics," *Front. Mod. Opt.* **24**, 189–205 (2016).
- ¹⁷⁷Z. Yang, M. Jahanbozorgi, D. Jeong, S. Sun, O. Pfister, H. Lee, and X. Yi, "A squeezed quantum microcomb on a chip," *Nat. Commun.* **12**, 4781 (2021); [arXiv:2103.03380](#).
- ¹⁷⁸V. Ansari, J. M. Donohue, M. Allgaier, L. Sansoni, B. Brecht, J. Roslund, N. Treps, G. Harder, and C. Silberhorn, "Tomography and purification of the temporal-mode structure of quantum light," *Phys. Rev. Lett.* **120**, 213601 (2018); [arXiv:1607.03001](#).
- ¹⁷⁹J. M. Donohue, V. Ansari, J. Řeháček, Z. Hradil, B. Stoklasa, M. Paúr, L. L. Sánchez-Soto, and C. Silberhorn, "Quantum-limited time-frequency estimation through mode-selective photon measurement," *Phys. Rev. Lett.* **121**, 090501 (2018); [arXiv:1805.02491](#).
- ¹⁸⁰V. Ansari, B. Brecht, J. Gil-Lopez, J. M. Donohue, J. Řeháček, Z. Hradil, L. L. Sánchez-Soto, and C. Silberhorn, "Achieving the ultimate quantum timing resolution," *PRX Quantum* **2**, 010301 (2021); [arXiv:2009.01069](#).
- ¹⁸¹In a quadrature-squeezed state,²⁰ $n = \sinh^2(r) = \exp(-2r) + \exp(2r) - 1/2$. As $r \rightarrow \infty$, $n \rightarrow \exp(2r)$. Therefore, $\sigma_{\Delta, TM} \propto \exp(-r)/[n((1/T_0)^2 + v_0^2)^{1/2}] \rightarrow \exp(-r)/[\exp(r)[(1/T_0)^2 + v_0^2]^{1/2}] = 1/[n((1/T_0)^2 + v_0^2)^{1/2}]$.
- ¹⁸²B. Dong, M. Dumont, O. Terra, H. Wang, A. Netherton, and J. E. Bowers, "Broadband quantum-dot frequency-modulated comb laser," *Light Sci. Appl.* **12**, 182 (2023); [arXiv:2306.15125](#).
- ¹⁸³Using the formula $-10 \log_{10}(1/5) \approx 7$ dB, where it is assumed that the standard quantum limit noise is normalized to 1.
- ¹⁸⁴R. K. Gosalia, R. Malaney, R. Aguinaldo, and J. Green, "Quantum super-resolution with balanced homodyne detection in low-earth-orbit," *Laser Phys.* **34**, 025201 (2023); [arXiv:2306.06541](#).
- ¹⁸⁵T. Song, Q. Wang, M. W. Wu, T. Ohtsuki, M. Gurusamy, and P. Y. Kam, "Impact of pointing errors on the error performance of intersatellite laser communications," *J. Lightwave Technol.* **35**, 3082–3091 (2017).
- ¹⁸⁶L. Zhang, J. Dai, C. Li, J. Wu, J. Jia, and J. Wang, "Design and in-orbit test of a high accuracy pointing method in satellite-to-ground quantum communication," *Opt. Express* **28**, 8291–8307 (2020).
- ¹⁸⁷A. Madni, N. Bradley, D. Cervantes, D. Eldred, D. Oh, D. Mathews, and P. C. Lai, "Pointing error budget development and methodology on the Psyche project," in *2021 IEEE Aerospace Conference (IEEE, 2021)*, pp. 1–18.

- ¹⁸⁸N. Shettell, W. J. Munro, D. Markham, and K. Nemoto, “Practical limits of error correction for quantum metrology,” *New J. Phys.* **23**, 043038 (2021); [arXiv:2101.02823](#).
- ¹⁸⁹G. Frascella, S. Agne, F. Y. Khalili, and M. V. Chekhova, “Overcoming detection loss and noise in squeezing-based optical sensing,” *npj Quantum Inf.* **7**, 72 (2021); [arXiv:2005.08843](#).
- ¹⁹⁰Y. Shaked, Y. Michael, R. Z. Vered, L. Bello, M. Rosenbluh, and A. Pe’er, “Lifting the bandwidth limit of optical homodyne measurement with broadband parametric amplification,” *Nat. Commun.* **9**, 609 (2018).
- ¹⁹¹E. Knyazev, F. Y. Khalili, and M. V. Chekhova, “Overcoming inefficient detection in sub-shot-noise absorption measurement and imaging,” *Opt. Express* **27**, 7868–7885 (2019); [arXiv:1810.08115](#).
- ¹⁹²C. Yue, J. Li, J. Sun, R. Zhu, X. Hou, X. Zhang, L. Liu, and W. Chen, “Homodyne coherent optical receiver for intersatellite communication,” *Appl. Opt.* **57**, 7915–7923 (2018).
- ¹⁹³M. Protte, T. Schapeler, J. Sperling, and T. J. Bartley, “Low-noise balanced homodyne detection with superconducting nanowire single-photon detectors,” *Optica Quantum* **2**, 1–6 (2024); [arXiv:2307.16672](#).
- ¹⁹⁴C. Peuntinger, B. Heim, C. R. Müller, C. Gabriel, C. Marquardt, and G. Leuchs, “Distribution of squeezed states through an atmospheric channel,” *Phys. Rev. Lett.* **113**, 060502 (2014); [arXiv:1402.6290](#).
- ¹⁹⁵A. Belsley, “Quantum-enhanced absorption spectroscopy with bright squeezed frequency combs,” *Phys. Rev. Lett.* **130**, 133602 (2023); [arXiv:2209.15628](#).
- ¹⁹⁶N. Picqué and T. W. Hänsch, “Frequency comb spectroscopy,” *Nat. Photonics* **13**, 146–157 (2019).
- ¹⁹⁷H. Shi, Z. Chen, S. E. Fraser, M. Yu, Z. Zhang, and Q. Zhuang, “Entanglement-enhanced dual-comb spectroscopy,” *npj Quantum Inf.* **9**, 91 (2023); [arXiv:2304.01516](#).
- ¹⁹⁸E. Russell, A. A. Ruth, B. Corbett, and F. C. Garcia Gunning, “Tunable dual optical frequency comb at 2 μm for CO₂ sensing,” *Opt. Express* **31**, 6304–6313 (2023).
- ¹⁹⁹K. M. Kwan, M. J. Yap, J. Qin, D. W. Gould, S. S. Y. Chua, J. Junker, V. B. Adya, T. G. McRae, B. J. J. Slagmolen, and D. E. McClelland, “Amplified squeezed states: Analyzing loss and phase noise,” *Class. Quantum Grav.* **41**, 205005 (2024).
- ²⁰⁰H. Wu, J. Ke, P.-P. Wang, Y.-J. Tan, J. Luo, and C.-G. Shao, “Arm locking using laser frequency comb,” *Opt. Express* **30**, 8027–8048 (2022); [arXiv:2109.02642](#).
- ²⁰¹B. Corcoran, M. Tan, X. Xu, A. Boes, J. Wu, T. G. Nguyen, S. T. Chu, B. E. Little, R. Morandotti, A. Mitchell, and D. J. Moss, “Ultra-dense optical data transmission over standard fibre with a single chip source,” *Nat. Commun.* **11**, 2568 (2020).
- ²⁰²Y. Shimizu, H. Matsukuma, and W. Gao, “Optical angle sensor technology based on the optical frequency comb laser,” *Appl. Sci.* **10**, 4047 (2020).
- ²⁰³Following Ref. 15, the ranging precision, $\sigma_R = \Delta R / (2 \ln 2 \sqrt{\eta n_s})$ where $C = 1$, $\Delta R = 52.6 \mu\text{m}$, $\eta = 1$ and $n_s = 108$ in our example. The ranging uncertainty for the quantum case would ideally scale as $\sigma_{R,Q} = \Delta R / (2 \ln 2 \sqrt{\eta n_s})$.